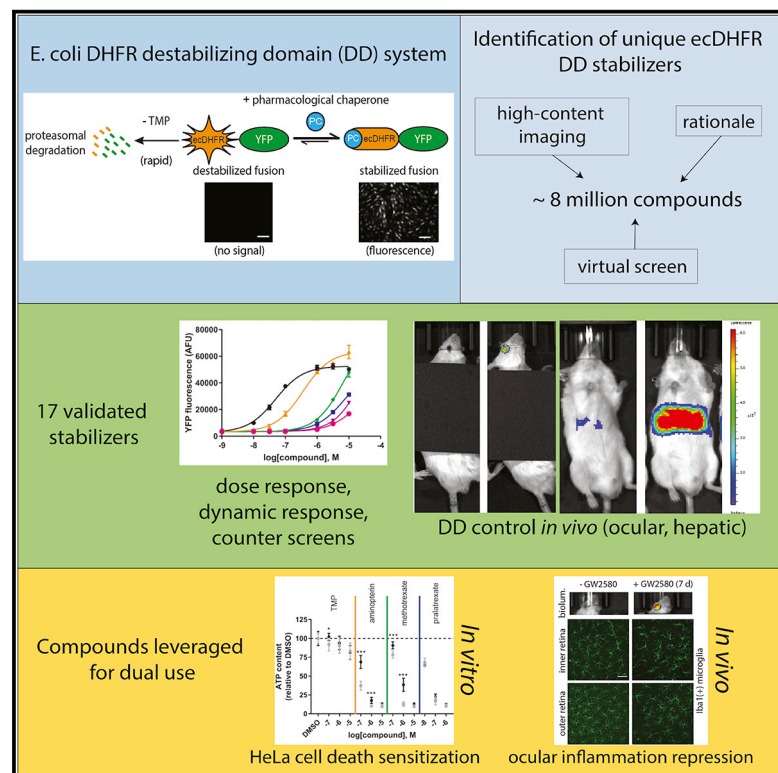


Cell Chemical Biology

Simultaneous Control of Endogenous and User-Defined Genetic Pathways Using Unique ecDHFR Pharmacological Chaperones

Graphical Abstract



Authors

Prerana Ramadurgum, DaNae R. Woodard, Steffi Daniel, ..., Peter M. Douglas, Bruce A. Posner, John D. Hulleman

Correspondence

john.hulleman@utsouthwestern.edu

In Brief

Ramadurgum et al. identify 17 new stabilizers of the *E. coli* dihydrofolate reductase (ecDHFR) destabilizing domain (DD) and validate them both *in vitro* and *in vivo* (mouse ocular and hepatic tissue). They also demonstrate the ability of these compounds to simultaneously control endogenous (stabilizer-defined) and user-defined (ecDHFR-DD-based) pathways.

Highlights

- Identification of 17 new ecDHFR DD stabilizers, dose responses, counter screens
- Dissection of minimal chemical and molecular requirements for ecDHFR DD stabilization
- HeLa cell death sensitization by concomitant hDHFR inhibition and dnHSF1 stabilization
- Simultaneous repression of ocular microglia and ecDHFR DD stabilization *in vivo*

Simultaneous Control of Endogenous and User-Defined Genetic Pathways Using Unique ecDHFR Pharmacological Chaperones

Prerana Ramadurgum,¹ DaNae R. Woodard,¹ Steffi Daniel,¹ Hui Peng,¹ Prema L. Mallipeddi,² Hanspeter Niederstrasser,² Melina Mihelakis,³ Viet Q. Chau,¹ Peter M. Douglas,³ Bruce A. Posner,² and John D. Hulleman^{1,4,5,*}

¹Department of Ophthalmology, University of Texas Southwestern Medical Center, 5323 Harry Hines Boulevard, Dallas, TX, USA

²Department of Biochemistry, University of Texas Southwestern Medical Center, 5323 Harry Hines Boulevard, Dallas, TX, USA

³Department of Molecular Biology, University of Texas Southwestern Medical Center, 5323 Harry Hines Boulevard, Dallas, TX, USA

⁴Department of Pharmacology, University of Texas Southwestern Medical Center, 5323 Harry Hines Boulevard, Dallas, TX, USA

⁵Lead Contact

*Correspondence: john.hulleman@utsouthwestern.edu

<https://doi.org/10.1016/j.chembiol.2020.03.006>

SUMMARY

Destabilizing domains (DDs), such as a mutated form of *Escherichia coli* dihydrofolate reductase (ecDHFR), confer instability and promote protein degradation. However, when combined with small-molecule stabilizers (e.g., the antibiotic trimethoprim), DDs allow positive regulation of fusion protein abundance. Using a combinatorial screening approach, we identified and validated 17 unique 2,4-diaminopyrimidine/triazine-based ecDHFR DD stabilizers, at least 15 of which were ineffective antibiotics against *E. coli* and *S. aureus*. Identified stabilizers functioned *in vivo* to control an ecDHFR DD-firefly luciferase in the mouse eye and/or the liver. Next, stabilizers were leveraged to perform synergistic dual functions *in vitro* (HeLa cell death sensitization) and *in vivo* (repression of ocular inflammation) by stabilizing a user-defined ecDHFR DD while also controlling endogenous signaling pathways. Thus, these newly identified pharmacological chaperones allow for simultaneous control of compound-specific endogenous and user-defined genetic pathways, the combination of which may provide synergistic effects in complex biological scenarios.

INTRODUCTION

Destabilizing domains (DDs) are unique chemical biology tools that enable the positive regulation of protein abundance through the use of a small-molecule pharmacological chaperone (Figure 1A) (Banaszynski et al., 2006; Iwamoto et al., 2010). The two primary DD systems used in biomedical research are (1) the FK506- and rapamycin-binding protein (FKBP12, stabilized by the synthetic ligand, Shd1 [Banaszynski et al., 2006]) and (2) the *E. coli* dihydrofolate reductase domain (ecDHFR, stabilized by the antibiotic, trimethoprim [TMP] [Iwamoto et al., 2010]). Yet, in theory, DDs can be generated through destabilizing mutagenesis of any protein and identification of a stabilizing ligand

(Miyazaki et al., 2012). The conventional DDs (FKBP12 and ecDHFR) have been successfully used in a number of biological and chemical biology applications ranging from gene editing (Maji et al., 2017; Manna et al., 2019) to controlling stress-responsive signaling (Chen et al., 2014; Cooley et al., 2014; Ryno et al., 2014), inflammation (Vu et al., 2017), and neuroprotection (Quintino et al., 2013). Previously, a number of groups have used DDs to regulate protein abundance *in vivo*, primarily in the brain (Banaszynski et al., 2006; Iwamoto et al., 2010; Quintino et al., 2013, 2018; Sando et al., 2013; Tai et al., 2012), whereas our focus has been on utilizing such systems in the mouse eye (Datta et al., 2019) using the canonical stabilizing ligand of the ecDHFR DD, TMP (Datta et al., 2018), or derivatives thereof (Peng et al., 2019).

While TMP has advantageous pharmacological properties such as central nervous system penetration, *in vivo* stability, and low nanomolar potency for ecDHFR, it is likely not the only compound that can bind to and stabilize the ecDHFR DD. In fact, there is a noticeable absence of alternative pharmacological chaperones that have been validated in this regard despite the abundance of known DHFR inhibitors and TMP analogs. As a proof of principle that TMP is not the only small molecule that can stabilize an ecDHFR DD, we recently demonstrated that a TMP derivative, 14a (MCC8529), which contains a linker and dansyl fluorophore added to the 4' position of the TMP phenyl ring, can also stabilize ocular and liver-based destabilized domains. However, unlike TMP, 14a does not confer antibiotic properties (Peng et al., 2019). Use of alternative non-antibiotic ecDHFR DD stabilizers, such as 14a, increase the likelihood of utilization of the ecDHFR DD *in vivo* as a potential gene therapy system in which a stabilizer would be required to be administered long term and would ideally not affect the gut microbiome. In contrast, prolonged use of antibiotic stabilizers, such as TMP, have the potential to cause alterations in the gut microbiome which may skew or confound analyses (Baim et al., 2019; Horai and Caspi, 2019; Kho and Lal, 2018). Additionally, newly identified compounds may have unique tissue distribution/pharmacokinetic/dynamic properties and/or inherently target attractive cellular signaling pathways when compared with the canonical stabilizer, TMP.

Here, we established a cell-based high-content imaging assay to identify potential ecDHFR DD stabilizing compounds

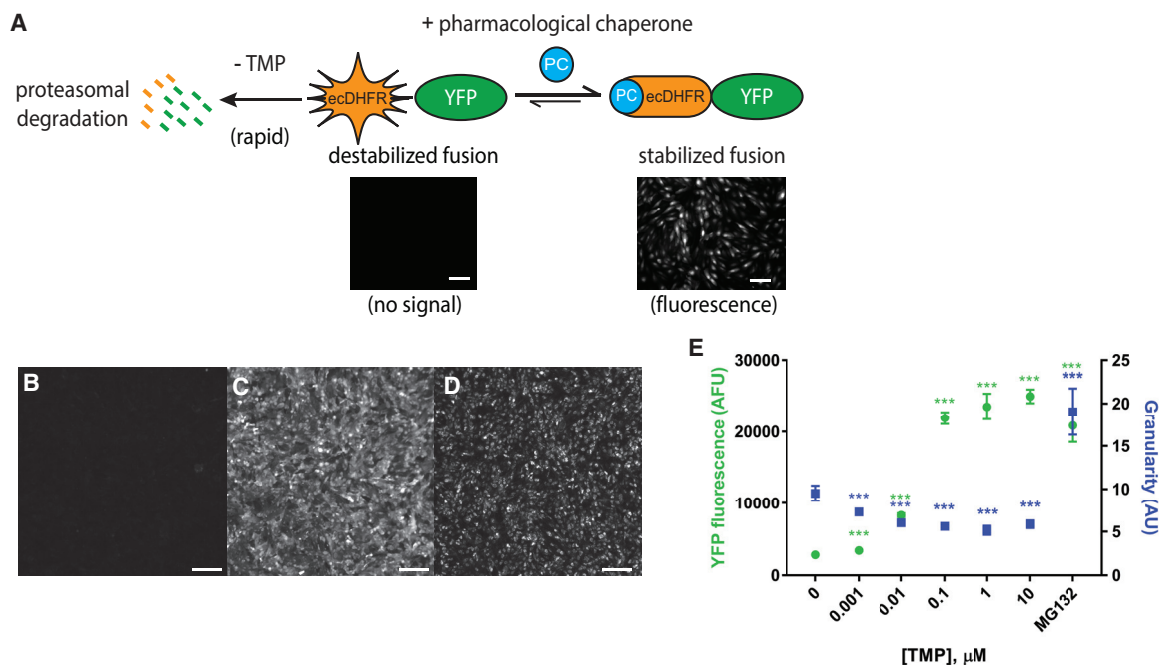


Figure 1. Schematic and Performance of a High-Content-Based Approach to Identify Chemical Stabilizers of an ecDHFR-Based Destabilizing Domain

(A) Schematic of the generalized strategy for regulating protein abundance using an ecDHFR destabilizing domain (DD).

(B–D) Representative images of wells obtained during high-content screening of ARPE-19 ecDHFR.YFP cells. Cells were treated with DMSO (B), TMP (C, 1 μ M, positive control) or MG132 (D, 10 μ M, false positive) for 24 h. Scale bars, 200 μ m.

(E) YFP fluorescence and image granularity as a function of TMP dose response or MG132 treatment. $n = 3$ (technical triplicates [separate wells]), mean \pm SD, *** $p < 0.001$, t test relative to DMSO control.

in an unbiased fashion. The common pharmacophore of newly identified stabilizers was elucidated, and its molecular interactions within the ecDHFR DD required for stabilization were identified. Subsequently, using rational and virtual screening approaches, we expanded the number of verified stabilizers more than 2-fold. The newly identified molecules can stabilize ecDHFR DDs *in vivo* in the eye and/or liver and offer the ability to exert dual functions, allowing for synchronous control of diverse endogenous signaling pathways and specific user-defined genetic pathways.

RESULTS

Establishment of a High-Content Imaging-Based Screen for DHFR Stabilizers

While TMP is the canonical ligand for stabilizing *E. coli* DHFR DDs (ecDHFR DDs), we speculated that additional, previously undiscovered small molecules might also be able to occupy the DHFR dihydrofolate binding pocket and therefore prevent ecDHFR DD degradation (Figure 1A). To identify these potential molecules, we screened an ARPE-19 cell line that constitutively expresses R12Y/G67S/Y100I ecDHFR (an N-terminal DD [Iwamoto et al., 2010]) fused to yellow fluorescent protein (YFP). When miniaturized in 384-well plates, under vehicle-treated conditions, virtually no YFP fluorescence is observed in these cells (Figure 1B), yet a very small amount of basal granular fluorescence can be detected. However, upon addition of TMP or MG-132, a proteasome inhibitor, a significant

increase in YFP fluorescence is observed (Figures 1C–E). In cells treated with TMP, we observed a concomitant decrease in basal YFP granularity due to promotion of newly produced YFP as a soluble, cytosolic form (Figures 1C and 1E). Conversely, cells treated with MG-132, which does not promote ecDHFR.YFP stabilization but rather inhibits its degradation, significantly elevated both YFP fluorescence and the granularity index (Figures 1D and 1E). Based on these observations, we rationalized that pharmacological chaperones of the ecDHFR DD (i.e., increased YFP intensity and decreased granularity) could be distinguished from potential false positives that inhibit proteasomal degradation (i.e., increased YFP intensity and increased granularity). Next, we screened 3,584 diverse compounds in a high-content imaging screen (HCS). The average Z' score across all 13 \times 384-well plates was 0.84 ± 0.10 (1 μ M TMP as the high control, DMSO as the low control), indicating excellent performance. Results from a representative 384-well plate are shown in Figures S1A and S1B.

HCS Identifies Stabilizers with a Minimum 2,4-Diaminopyrimidine/Aryl Group Pharmacophore

Screening of 3,584 compounds (5 μ M final concentration, 24 h treatment) yielded an initial series of ten hit compounds that demonstrated a YFP fluorescence increase of $\geq 20\%$ of the TMP-positive control and a $\geq 35\%$ reduction in granularity compared with vehicle-treated cells. Two of the hits, F16 and pyruvium pamoate, were determined to be fluorescent false

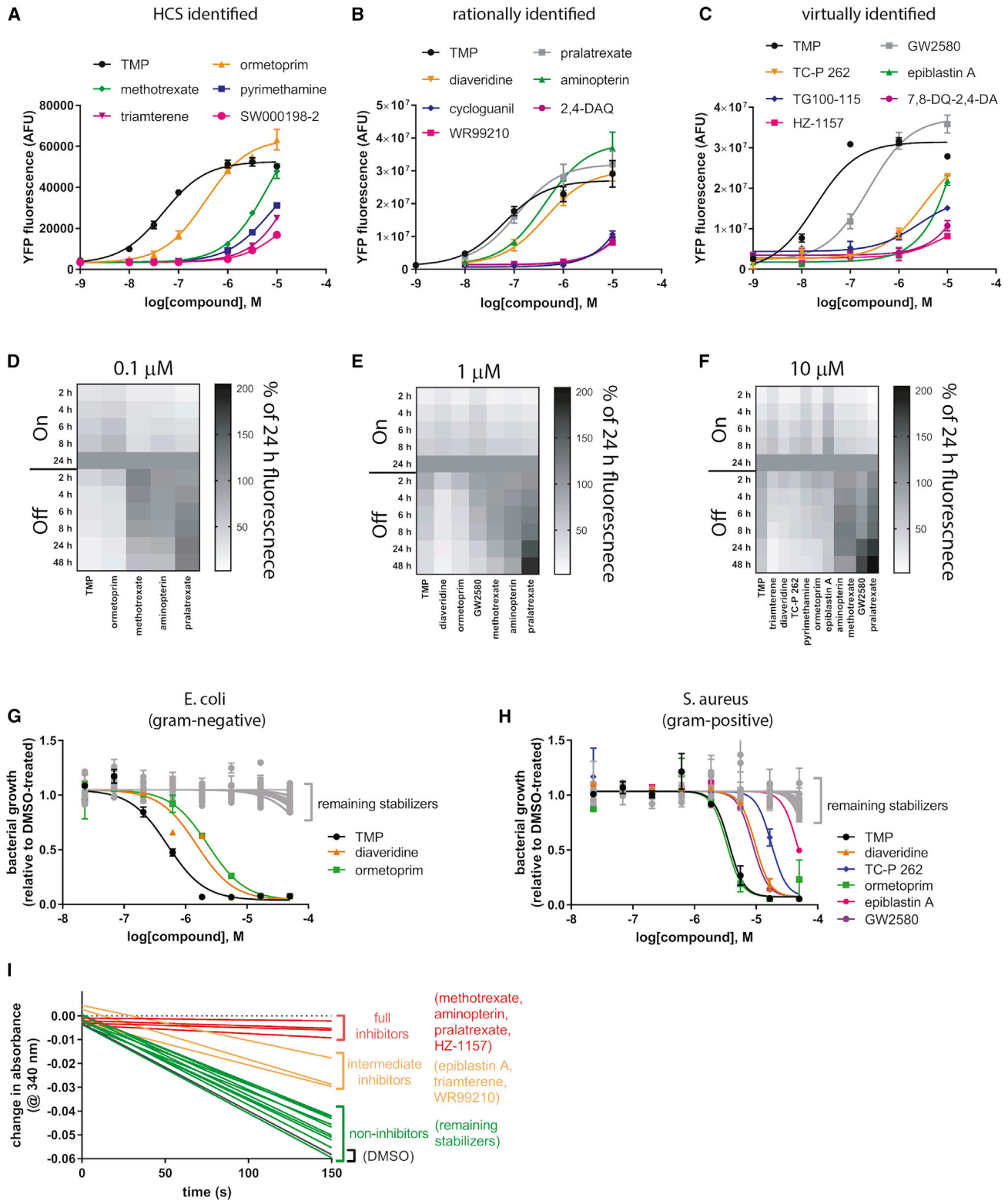


Figure 2. ecDHFR.YFP Stabilizers Identified through a Combination of Screening Methods

(A) High-content imaging screen (HCS) of 3,584 compounds identified five new stabilizers (in addition to TMP) that elevated YFP fluorescence and reduced YFP granularity (relative to DMSO control) and were dose dependent. n = 3 (technical triplicates [separate wells]), mean ± SD.

(B) Rationally identified ecDHFR DD stabilizers based on the pharmacophore identified in the HCS hit compounds and not present in inactive compounds (Figure S4) are capable of dose-dependently stabilizing ecDHFR.YFP to varying degrees. n = 3 independent experiments, mean ± SD

(legend continued on next page)

positives based on follow-up studies in ARPE-19 cells lacking ecDHFR.YFP and were therefore excluded. Thus, our hit rate was 8 out of 3,584 compounds or 0.22%, demonstrating a highly selective, non-promiscuous assay. One compound, methotrexate, was identified as a hit in three separate libraries, reducing the number of unique hit compounds to 6 out of 3,584. Of these six unique hit molecules (Figures 2A and S2), four were well-known DHFR inhibitors: TMP (an ecDHFR inhibitor (Reisberg et al., 1966)), ormetoprim (a TMP analog), methotrexate (a broad-spectrum DHFR inhibitor), and pyrimethamine (an antiparasitic *Plasmodium falciparum* DHFR inhibitor [Jaswant et al., 1951]). The remaining two hit compounds were triamterene, a Food and Drug Administration (FDA)-approved potassium-sparing diuretic (Crosley et al., 1962), and a newly identified molecule, SW000198-2 (PubChem compound CID: 1069125) that resembles the scaffold of antiparasitics such as cycloguanil and WR99210 (Figure S2). All hit compounds are listed in Figure S2, whereas select hit compounds with diverse inherent functions are highlighted in Table 1. Initial HCS-identified hit compounds were verified in a dose-response assay with a fresh aliquot of compound, where all molecules produced a dose-dependent increase in YFP fluorescence with half-maximal active concentrations (AC_{50}) ranging from 49 nM (TMP) to >10 μ M (triamterene, SW000198-2; Figures 2A and S2; Table 1). Finally, ecDHFR.YFP stabilization was confirmed in a secondary assay, which directly measured protein levels after treatment with 10 μ M of the hit compound (Figures S3A and S3B). Interestingly, all hit compounds contained, at minimum, a 2,4-diaminopyrimidine (2,4-DAP) ring structure linked to an aryl group. SW000198-2 was the only triazine-containing compound identified in the initial screen.

Defining the Necessary versus Sufficient Chemical Structure for ecDHFR DD Stabilization

Given the low hit percentage of our initial screen, we speculated that the binding pocket of our destabilized ecDHFR specifically requires a 2,4-DAP ring (or similar structure) conjugated to an additional aryl group. Yet we were unsure whether such a structure was necessary versus sufficient for stabilization. To address this question, we rationally identified compounds containing slight modifications of the predicted 2,4-DAP/aryl group pharmacophore at select positions in their chemical structure (Figure S4) and tested whether they could regulate ecDHFR.YFP abundance (10 μ M final concentration, 24 h treatment). The 2,4-DAP structure alone or in combination with a carbaldehyde modification (2,4-diaminopyrimidine-5-carbaldehyde [2,4-DAP-5C]) were insufficient to stabilize ecDHFR.YFP (Figures S4A and S4B). Absence of the 4'

amine group (i.e., 2-aminoquinazoline [2-AQ]), or replacement of it with an oxygen (i.e., 2-amino-3H-quinazolin-4-one [2-AQ-4O]), dihydrofolic acid, pemetrexed, or raltitrexed) did not allow for stabilization of ecDHFR.YFP either (Figures S4A and S4B), even if the molecule otherwise closely resembled a hit compound (i.e., compare methotrexate [Figure S2] with dihydrofolic acid, pemetrexed, or raltitrexed [Figure S4]). Additionally, proguanil, a prodrug of cycloguanil (similar to pyrimethamine), had no stabilization capabilities at the tested concentration of 10 μ M (Figures S4A and S4B). Based on these observations, we concluded that a 2,4-DAP and an aryl group originating from the 1 or 6 position in the pyrimidine ring was the minimum pharmacophore required for stabilization of ecDHFR DDs.

Rationally Identified Molecules Stabilize ecDHFR.YFP

Based on our insight into the molecular requirements of ecDHFR DD stabilization, we manually searched the literature for commercially available small molecules that, at minimum, contained the 2,4-DAP/aryl pharmacophore. The TMP analog, diaveridine (Figure 2B), dose-dependently stabilized ecDHFR.YFP in a manner similar to that of ormetoprim (compare Figure 2A [AC_{50} = 0.36 μ M] with Figure 2B [AC_{50} = 0.37 μ M]), but not as efficiently as TMP at lower concentrations (Figure 2B). Methotrexate analogs such as pralatrexate (DeGraw et al., 1993) and aminopterin (Table 1 and Figure S2) readily stabilized ecDHFR.YFP in a dose-dependent manner (Figure 2B). In fact, pralatrexate was the only compound that approached the potency and efficacy of TMP for stabilizing ecDHFR.YFP (AC_{50} = 0.11 μ M). Cycloguanil and WR99210, which share a similar structure to pyrimethamine (although WR99210 was one of three verified hits with a triazine ring, not a pyrimidine backbone), also stabilized ecDHFR.YFP (Figures 2B and S2), but were relatively ineffective when compared with TMP, pralatrexate, diaveridine, or aminopterin (Figure 2B, AC_{50} > 10 μ M). The smallest identified stabilizer was 2,4-diaminoquinazoline (2,4-DAQ, Figures 2B and S2), a compound similar to one previously discovered to have weak ecDHFR-binding abilities (Carroll et al., 2012). Finally, we confirmed the stabilization of ecDHFR.YFP protein levels in cells treated with each of the rationally identified, commercially available compounds (Figures S3C and S3D).

Virtual Database Screening Identifies Potential Stabilizers with Unique Functions

Given our increasing knowledge of the structural requirements of ecDHFR DD stabilizers, we next sought to identify already existing compounds that contained the minimal stabilizing structure through virtual screening of existing chemical

(C) Virtual screening of two chemical databases identifies compounds with diverse functions as ecDHFR DD stabilizers. n = 3 independent experiments, mean \pm SD.

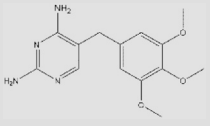
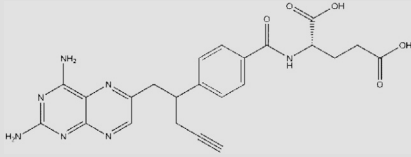
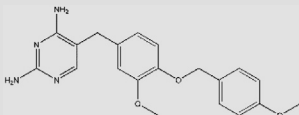
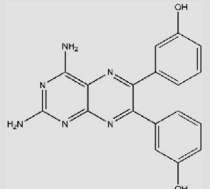
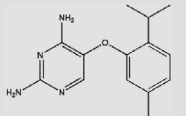
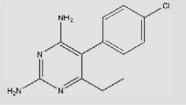
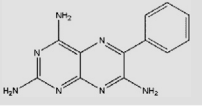
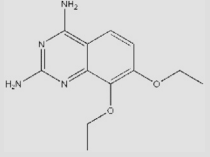
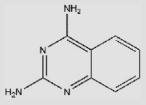
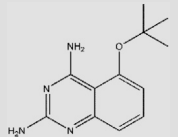
(D–F) Dynamic stabilization and washout of select hit compounds at 0.1 μ M (D), 1 μ M (E), and 10 μ M (F). Representative data of three independent experiments.

(G) Fifteen out of 17 newly identified stabilizers have no anti-bacterial properties in Gram-negative BW25113 wild-type *E. coli*, in contrast to TMP or TMP derivatives, diaveridine or ormetoprim. Representative curves of three independent experiments.

(H) Thirteen out of 17 identified stabilizers have no significant anti-bacterial properties in Gram-positive RN4220 *S. aureus* at concentrations up to 50 μ M. Representative curves of three independent experiments.

(I) An enzymatic inhibition assay identifies unknown intermediate and full inhibitors of human DHFR at 1 μ M. Representative linear regression of at least two independent experiments.

Table 1. Compound Information about Select Pharmacological Chaperones of eCDHFR DDs with Diverse Functions

Compound	Structure	AC ₅₀ (nM)	Primary Target	Reference
TMP		19–52	<i>Escherichia coli</i> DHFR	Reisberg et al., 1966
Pralatrexate		110	<i>Homo sapiens</i> DHFR	DeGraw et al., 1993
GW2580		240	cFMS kinase	Conway et al., 2005
TG100-115		2,500	PI3Kγ/δ	Doukas et al., 2006
TC-P 262		3,400	P2X ₃ and P2X _{2/3}	Ballini et al., 2011
Pyrimethamine		7,200	protozoal DHFR	Jaswant et al., 1951
Triamterene		>10,000	ENaC	Crosley et al., 1962
7,8-DQ-2,4-DA		>10,000	GCCase PC	Tropak et al., 2008
2,4-DAQ		>10,000	uncertain	N/A
HZ-1157		>10,000	HCV NS3/4A protease	Yu et al., 2014

databases. Approximately 7 million compounds from MolPort (<https://www.molport.com>) and ~8 million compounds from eMolecules (<https://emolecules.com>) were screened to identify compounds that had both a 2,4-DAP moiety combined with an aryl group extending from the 1 or 6 position in the pyrimidine

ring. We identified 136 unique small molecules that fit this profile (Table S1). Intriguingly, a number of these molecules were previously not characterized as eCDHFR or more broadly as DHFR inhibitors, but instead were identified as having multiple functions ranging from purinergic receptor P2X_{2/3}

antagonist (TC-P 262 [Ballini et al., 2011]) to glucocerebrosidase (GCase) pharmacological chaperone (7,8-dithoxy-quinazoline-2,4-diamine, [7,8-DQ-2,4-DA] [Tropak et al., 2008]) to phosphoinositide 3-kinase γ/δ (PI3K γ/δ) inhibitor (TG100-115 [Doukas et al., 2006]) to cFMS receptor tyrosine kinase inhibitor (GW2580 [Conway et al., 2005]). We tested a series of six representative compounds (Figure 2C) from this group and found that they could all stabilize ecDHFR.YFP to varying degrees ranging from $AC_{50} = 0.24 \mu\text{M}$ (GW2580) to $AC_{50} > 10 \mu\text{M}$ (7,8-DQ-2,4-DA, HZ-1157; Figure 2C and Table 1), and stabilization at $10 \mu\text{M}$ was confirmed by western blotting (Figures S3E and S3F). Interestingly, a test of two additional molecules identified from the virtual screen, RG3039 (Butchbach et al., 2010) and D156844 (Harris and Butchbach, 2015), inhibitors of the mRNA decapping scavenger enzyme, with promise for the treatment of spinal muscular atrophy, failed to demonstrate an ability to stabilize the ecDHFR DD (Figure S5). Absence of stabilization in this context is possibly due to steric hindrance within the ecDHFR-binding pocket originating from extensive modification of the minimal pharmacophore (2,4-DAQ) at the C5 position of the aryl ring.

Identified Stabilizers Display Unique Dynamic Stabilization/Destabilization Compared with TMP

After validation of hit compound stabilizing effects after 24 h of treatment, we next determined how quickly and efficiently select compounds could stabilize ecDHFR.YFP, followed by destabilization after compound withdrawal. At relatively low concentrations ($0.1 \mu\text{M}$), TMP and ormetoprim demonstrated gradual “On” kinetics followed by quick “Off” kinetics 2–4 h after removal (Figure 1D). At 1 and $10 \mu\text{M}$, diaveridine and ormetoprim were able to stabilize similarly to TMP (Figures 2A and 2B), yet had noticeably quicker “Off” kinetics (Figures 2E and 2F). Thus, these two compounds, or other TMP derivatives, should be able to achieve more transient stabilization *in vivo* when compared with TMP. Surprisingly, human DHFR (hsDHFR) inhibitors methotrexate, aminopterin, and pralatrexate continued to stabilize ecDHFR, even 48 h post washout (Figure 2D), possibly due to inefficient metabolism in cell culture or stronger binding to ecDHFR. In fact, ecDHFR.YFP fluorescence for pralatrexate peaked at 48 h at all concentrations used (Figures 2D–2F). Yet, these observations may be drastically different *in vivo* where compounds can be more affected by tissue penetration, excretion, and metabolism.

The Majority of Newly Identified ecDHFR DD Stabilizers Lack Effective Antibiotic Properties

While TMP can promote ecDHFR DD protein abundance in the nanomolar range, one adverse property when used *in vivo* for controlling gene therapy strategies is that it is an antibiotic. Therefore, unnecessary use of TMP could not only promote antibiotic resistance (Toprak et al., 2011) but can also disrupt the gut microbiome after a single administration (Peng et al., 2019). We speculated that the newly identified ecDHFR DD stabilizers would not function as effective antibiotics to halt Gram-negative *E. coli* growth, and therefore may confer an additional advantage over TMP when used *in vivo*. In a standard bacterial growth assay, out of the 17 verified ecDHFR DD stabilizers, only TMP (minimal inhibitory concentration [MIC] $\sim 1.8 \mu\text{M}$) and

the two TMP derivatives, ormetoprim and diaveridine (MIC $\sim 16.6 \mu\text{M}$), demonstrated any antibiotic activity using concentrations up to $50 \mu\text{M}$ (Figure 2D).

We further tested the ability of the identified hit compounds to inhibit Gram-positive *S. aureus* growth and found that TMP and ormetoprim demonstrated the highest level of growth inhibition out of all compounds tested, with MICs of $\sim 16.6 \mu\text{M}$ (Figure 2H). Diaveridine, TC-P 262, and GW2580 also demonstrated growth inhibition properties with MICs of $\sim 50 \mu\text{M}$ (Figure 2H), a concentration that would be unlikely to be achieved *in vivo* for sustained periods of time. Finally, epiblastin A also reduced *S. aureus* proliferation beginning at $50 \mu\text{M}$, but did not completely inhibit growth at the concentrations tested (Figure 1H).

Some Hit Compounds Act as hsDHFR Inhibitors at High Concentrations

Inhibition of mammalian DHFR for any prolonged period of time would arguably be an unwanted side effect in most biological contexts, with the exception of potentially reducing cancer cell growth. We therefore screened all hit compounds for their ability to inhibit recombinant hsDHFR at $1 \mu\text{M}$. As expected, known hsDHFR inhibitors methotrexate, pralatrexate, and aminopterin completely inhibited hsDHFR activity (Figure 2I). Surprisingly, though, HZ-1157, a previously identified hepatitis C NS3/4A protease inhibitor (Yu et al., 2014), also fully inhibited hsDHFR at $1 \mu\text{M}$, raising concerns about the translatability of this compound for safely treating hepatitis C. Epiblastin A, WR99210, and triamterene intermediately inhibited hsDHFR at $1 \mu\text{M}$, in accordance with speculation from previous reports (Corcino et al., 1970; Illich et al., 2016) yet, intermediate inhibition of hsDHFR is sufficiently tolerated in humans to allow triamterene to become an FDA-approved drug as an antidiuretic agent (clinicaltrials.gov).

Molecular Modeling Identifies Unique ecDHFR Residues Responsible for Facilitating Small-Molecule Binding

To gain structural insight into small-molecule interactions that could be playing a role in stabilizing ecDHFR DD, we modeled the ecDHFR DD *in silico*, then docked the minimal stabilizer, 2,4-DAQ (Figure 3A) or inactive derivatives, 2-AQ (lacking the necessary 2,4-diamino moiety) or 2,4-DAP (lacking the necessary aryl moiety). The overall dock score indicated a stronger binding of the active 2,4-DAQ compound (-8.10 kcal/mol) compared with inactive compounds 2-AQ (-6.80 kcal/mol) or 2,4-DAP (-6.20 kcal/mol , Figure 3B). Specifically, the docked pose of 2,4-DAQ exhibits hydrogen-bond interactions with main-chain carbonyl groups of Ile5 and Ile94 as well as the Asp27 side chain. The amino group at position 2 in 2,4-DAQ and 2,4-DAP formed hydrogen-bonding interactions with the backbone carbonyl of Ile5 (Figure 3B). This same interaction was weaker in 2-AQ, which lacks the 2-position amino group (Figure 3B). Similarly, 2,4-DAQ and 2-AQ shared stronger interactions with Phe31, unlike 2,4-DAP, which lacks the aryl group, suggesting that this interaction is promoted by the aryl group on the small molecule, in accordance with suggestions from previous studies (Cao et al., 2018). Met16 and Ile94 provided unique, strong interactions with 2,4-DAQ in contrast to 2-AQ and 2,4-DAP (Figure 3B), which may suggest that these interactions occur only after engagement with other initial stabilizing interactions. Supporting this notion, Met16, which is in the

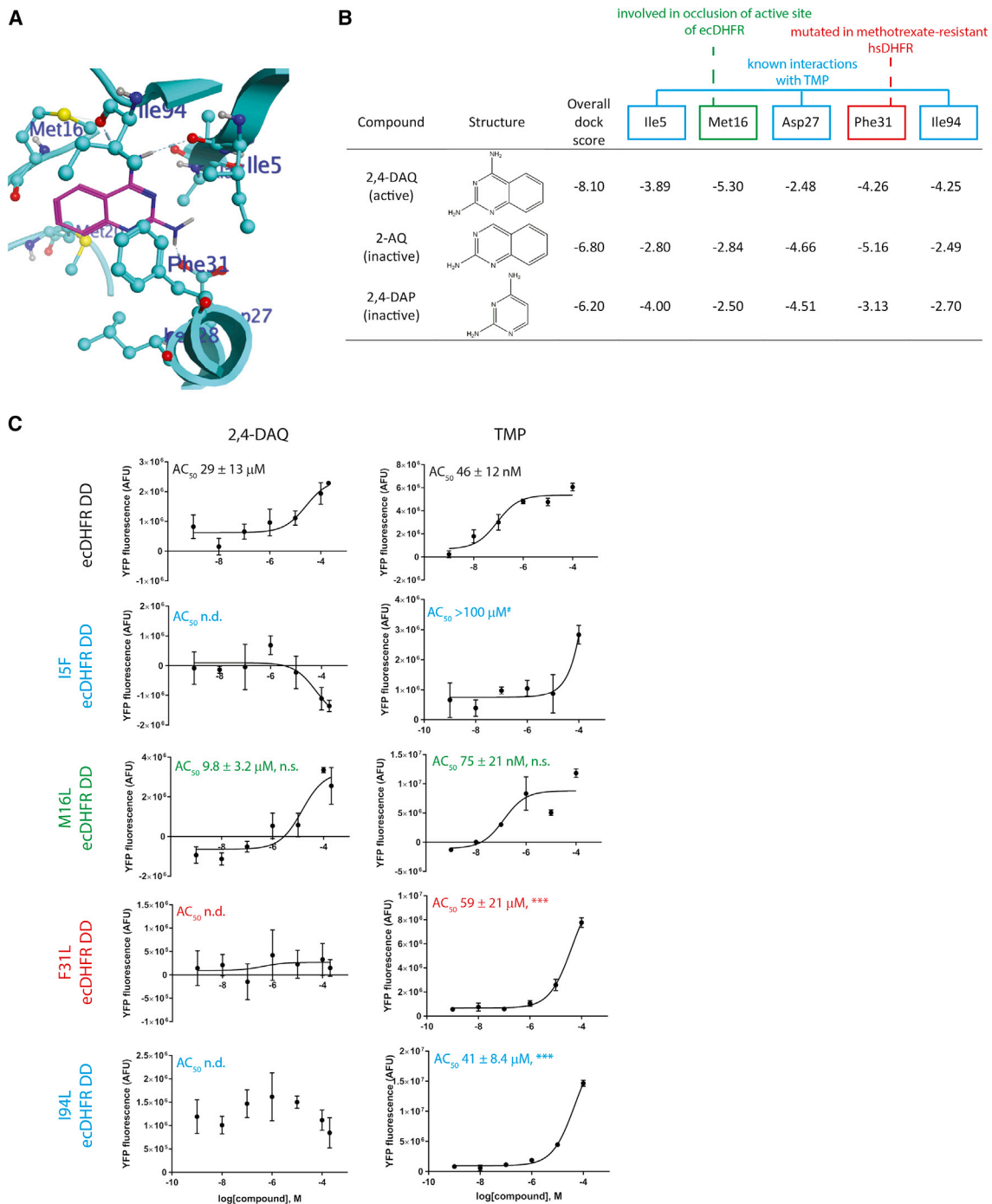


Figure 3. Modeling and Docking Studies Identify Known and Unique Interactions Necessary for Small-Molecule Binding to ecDHFR

(A) An *in silico* model of the R12Y/G67S/Y100I ecDHFR DD was generated based on wild-type ecDHFR bound to dihydrofolate (DHF) (PDB: 6CXK), followed by docking of the smallest active (2,4-DAQ, shown) or inactive compounds lacking the 2,4-diamino group (2-AQ) or extended aromatic structure (2,4-DAP) necessary for stabilization.

(B) Table of interaction energies (in kcal/mol) with key residues identified to be responsible for favorable binding of 2,4-DAQ versus 2-AQ and 2,4-DAP in the DHF binding pocket of the modeled ecDHFR DD.

(C) Dose-response stabilization curves of the indicated stable cells incubated with either 2,4-DAQ or TMP for 24 h followed by Celigo analysis. Representative data of ≥ 3 independent experiments performed in technical triplicates are presented. AC_{50} values are means \pm SEM of the independent experiments. *** $p < 0.001$, one-tailed t test assuming equal variance when compared with either 2,4-DAQ or TMP-treated control ecDHFR DD cells. n.s., not significant; n.d., not determined (response was negative or not reliable). $^{\#}$ Two out of three experiments performed with TMP-treated I5F cells yielded an $AC_{50} > 100 \mu\text{M}$.

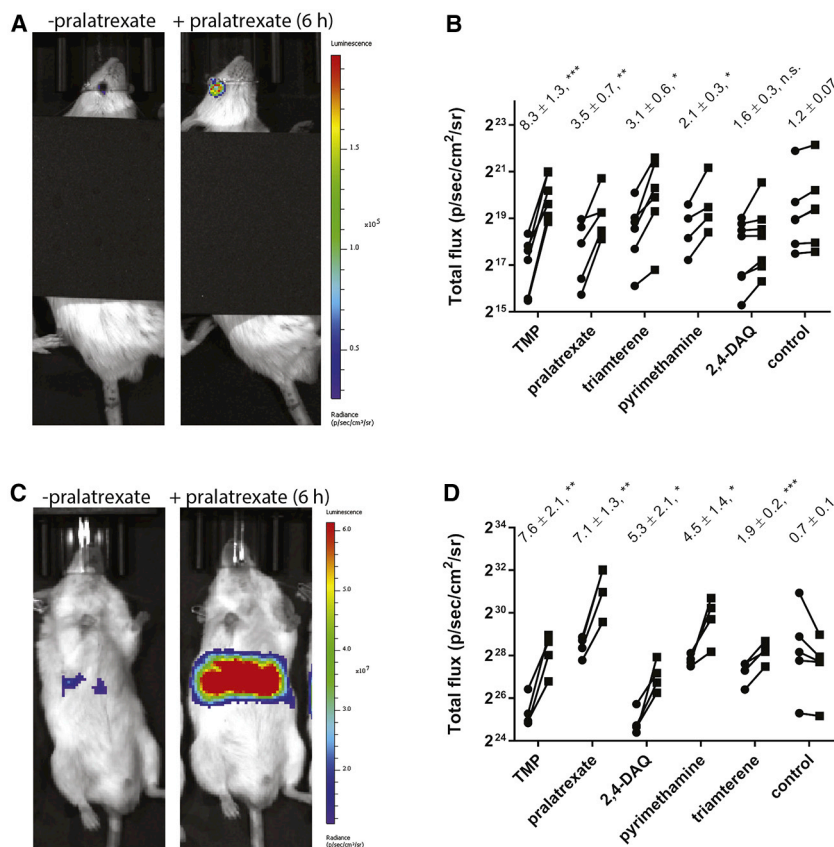


Figure 4. In Vivo Verification of Select Stabilizing Molecules in the Eye and Liver

Wild-type non-pigmented BALB/c mice were intravitreally (A) or intravenously (C) injected with adeno-associated virus encoding for ecDHFR firefly luciferase (ecDHFR.FLuc), assessed for baseline ocular/hepatic bioluminescence, and induced with 1 mg (50 mg/kg) of the indicated compound (via oral gavage). Bioluminescence was measured 6 h post gavage. Representative images of pralatrexate-treated mice are provided as examples (A and C). $n = 4-7$ mice per treatment. Mean fold change \pm SEM is shown (B and D). * $p < 0.05$, ** $p < 0.01$, *** $p < 0.001$, one-tailed t test versus control untreated mice. Note: a black tarp was used in (A) to block apparent background luminescence that can originate from the ear tag of the mice.

Met20 loop, a region known to play a critical role in ecDHFR enzymatic function and substrate binding (Boehr et al., 2006; Sawaya and Kraut, 1997), has been previously shown to occlude the ecDHFR active site upon transition from the closed state to occluded state (Mauldin et al., 2012). Interestingly, inactive compounds interacted more strongly with Asp27 than 2,4-DAQ, possibly due to a looser occupancy of the dihydrofolate binding pocket. Many of the interactions identified are consistent with previously reported complexes such as an *E. coli* DHFR/methotrexate complex (PDB: 1RA3) (Sawaya and Kraut, 1997) and a *Mycobacterium tuberculosis* DHFR in complex with cycloguanil (PDB: 4KNE) (Dias et al., 2014). In fact, three of the interacting residues (Ile5, Asp27, and Ile94) were known previously to interact via hydrogen bonding and/or van der Waals interactions with TMP (Lee et al., 2010; Li et al., 2000), and have been previously found to be mutated in TMP-resistant bacteria (Tamer et al., 2019). Furthermore, mutation of Phe31 has been found in methotrexate-resistant hsdHFR (Chunduru et al., 1994).

We verified the predicted stabilizing interactions by generating ARPE-19 cells stably expressing ecDHFR DD YFP variants (already containing the R12Y/G67S/Y100I triple mutation) mutated additionally at either Ile5 [I5F, previously identified as a TMP-resistant mutation [Tamer et al., 2019], Met16 [M16L], Phe31 [F31L], or Ile94 [I94L, also previously identified as a TMP-resistant mutation [Tamer et al., 2019]]) and treating them with either 2,4-DAQ or TMP. 2,4-DAQ stabilized the control ecDHFR DD with an $AC_{50} = 29 \pm 13 \mu\text{M}$ whereas TMP

stabilized ecDHFR DD with an $AC_{50} = 46 \pm 12 \text{ nM}$ (Figure 3C). Mutation of Ile5, Phe31, or Ile94 eliminated all responsiveness to 2,4-DAQ stabilization and significantly reduced TMP-mediated stabilization by ≥ 891 -fold (Figure 3C). In contrast, mutation of Met16 did not significantly disrupt 2,4-DAQ or TMP-based stabilization (Figure 3C). When these results are combined with the modeling, they suggest that indeed Ile5 may be the critical residue for interacting with the stabilizer's 2-position amine group whereas Phe31 may be critical for stabilization through potential π - π interactions with the aryl group. Subsequently, Ile94 may solidify compound mediated stabilization once both Ile5 and Phe31 have bound to the small molecule.

Representative Stabilizers Can Also Regulate ecDHFR DD Abundance In Vivo

Next, we evaluated whether four representative newly identified stabilizers (pyrimethamine, triamterene, pralatrexate, and 2,4-DAQ) could stabilize an ecDHFR DD reporter protein *in vivo* in the mouse eye (Figures 4A and 4B) or mouse liver (Figures 4C and 4D). All compounds were compared with the canonical stabilizer, TMP. After intravitreal injection of an rAAV2/2[MAX] (which targets the neural retina, with enhanced transduction of photoreceptors) encoding for ecDHFR DD firefly luciferase (ecDHFR.FLuc), mice were evaluated for baseline bioluminescent signal 1 day prior to treatment with compound (1 mg, 50 mg/kg, via oral gavage). Six hours after molecule administration, mice were again evaluated for bioluminescent ecDHFR.FLuc signal to determine the extent of ecDHFR stabilization. In the eye, TMP demonstrated the highest significant fold change in luminescence after treatment (8.3 ± 1.3 fold, Figure 4B), followed by pralatrexate (3.5 ± 0.7 fold, Figure 4B), triamterene (3.1 ± 0.6 fold, Figure 4B), and pyrimethamine (2.1 ± 0.7 fold, Figure 4B). 2,4-DAQ was not able to significantly promote ecDHFR.FLuc levels in the eye (1.6 ± 0.3 fold, Figure 4B), a fold change similar to that of untreated mice (1.2 ± 0.07 fold, Figure 4B).

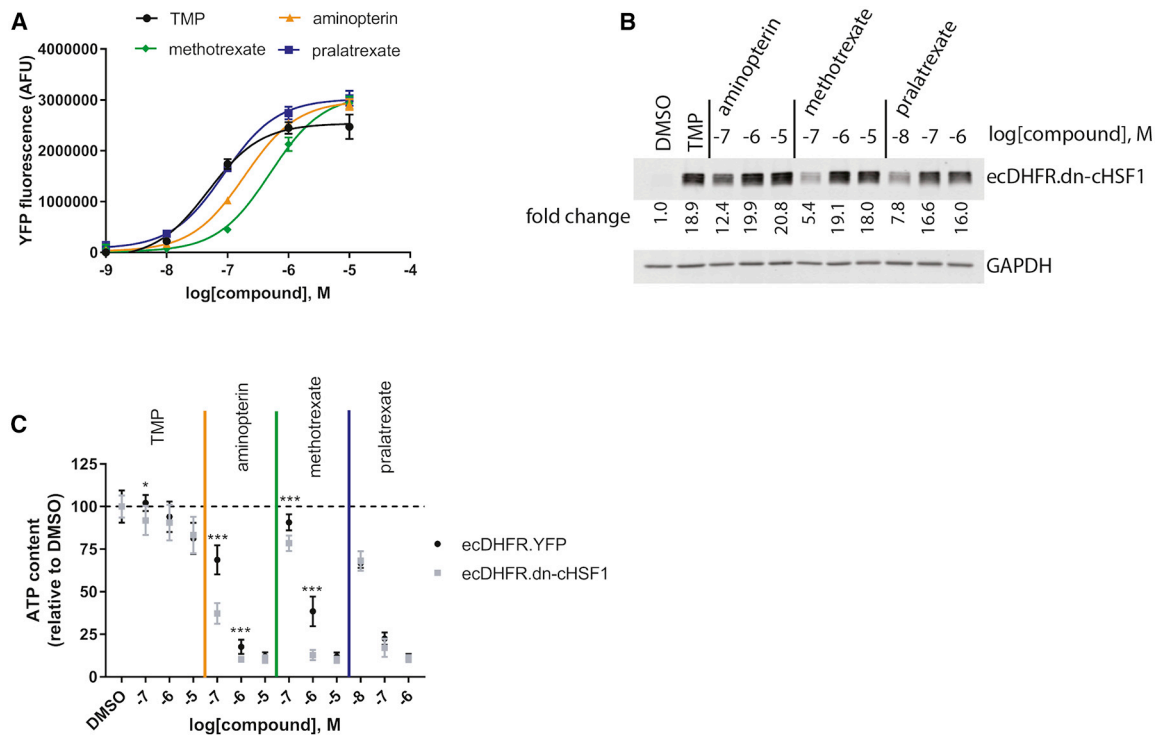


Figure 5. Newly Identified Stabilizers Can Be Leveraged for Simultaneous Targeting of Endogenous and User-Defined Genetic Pathways In Vitro

(A and B) Human DHFR (hsDHFR) inhibitors can be used to dose-dependently control ecDHFR.YFP (as determined by cellular fluorescence) (A) or ecDHFR.dn-cHSF1 (as determined by western blotting) (B) in HeLa Tet-On cells.

(C) Simultaneous hsDHFR inhibition and repression of heat-shock factor signaling synergistically compromises cancer cell viability. HeLa Tet-On cells expressing ecDHFR.YFP or ecDHFR.dn-cHSF1 were treated with the indicated compounds for 24 h followed by an ATP content assay (Cell-Titer-Glo 2.0). n = 3–4 independent experiments performed in biological triplicates; *p < 0.05, ***p < 0.001, two-tailed t test versus ecDHFR.dn-cHSF1.

Subsequently, we explored whether the same compounds could stabilize an ecDHFR DD systemically in the mouse liver. Mice were injected with an rAAV2/8 virus encoding for ecDHFR.FLuc via tail vein injection. After obtaining baseline readings, molecules were administered the following day (1 mg, 50 mg/kg, oral gavage) and mice were imaged 6 h later. TMP demonstrated the highest fold change in the liver, increasing the bioluminescent signal by 7.6 ± 2.1 fold (Figure 4D). The remaining compounds also significantly stabilized ecDHFR.FLuc, some at levels similar to TMP; pralatrexate (7.1 ± 1.3 fold), 2,4-DAQ (5.3 ± 2.1 fold), pyrimethamine (4.5 ± 1.4 fold), and triamterene (1.9 ± 0.2 fold, all from Figure 4D). Interestingly, aside from TMP, all compounds led to a higher level of stabilization in the liver (Figure 2D) than in the eye (Figure 2B), likely due to the fact that compounds are inherently more difficult to transport across the blood-brain barrier than the liver, where they accumulate and are metabolized by phase I/II enzymes. Thus, aside from the lack of significant regulation of 2,4-DAQ in the eye, all remaining selected compounds can be used for regulating ecDHFR DD abundance in the eye and more broadly in the body, likely with unique pharmacokinetic/pharmacodynamic properties. While these studies were performed at a single dose and time point, they clearly indicate that the majority of tested molecules can be leveraged for *in vivo* use. However, we acknowledge that additional experiments focused on ki-

netics of induction/reversal of the ecDHFR DD could provide important information regarding unique pharmacokinetics/pharmacodynamics for each of these compounds.

Identified Stabilizers Can Be Leveraged to Perform Dual Synergistic Functions

Given the wide variety of previously defined functions of the newly identified stabilizers (Table 1), we hypothesized that many of the compounds could be leveraged to achieve simultaneous regulation of endogenous signaling pathways while also controlling a user-defined genetically encoded pathway on an ecDHFR DD fusion protein. To test this hypothesis, we leveraged the hsDHFR inhibitors, aminopterin, methotrexate, and pralatrexate, which have been used as cancer treatments (Raimondi et al., 2019), to control an ecDHFR DD fused to a dominant negative version of heat-shock factor 1 (dn-cHSF1) (Moore et al., 2016), a transcription factor thought to be important for cancer growth (Dai and Sampson, 2016; Santagata et al., 2011). We validated the use of hsDHFR inhibitors for regulating ecDHFR.YFP and ecDHFR.dn-cHSF1 in stable HeLa cells (Figures 5A and 5B). Treatment of ecDHFR.dn-cHSF1 HeLa cells with TMP did not lower ATP content of the cells compared with ecDHFR.YFP-expressing control HeLa cells (Figure 5C), indicating that inhibition of HSF1 signaling alone was not sufficient to compromise cell viability. However, the combination of

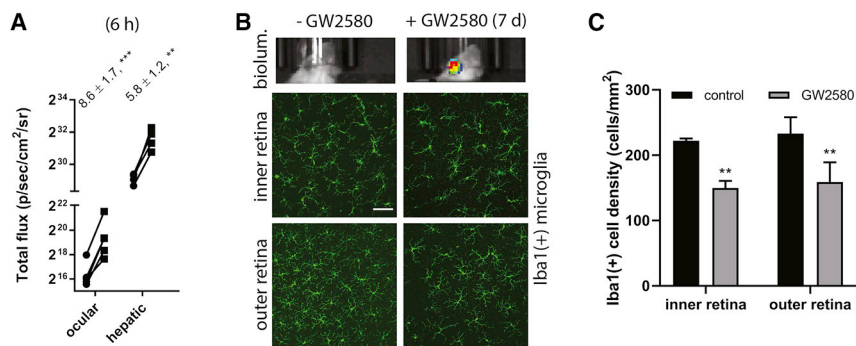


Figure 6. Newly Identified Stabilizers Can Be Leveraged for Simultaneous Targeting of Endogenous and User-Defined Genetic Pathways In Vivo

(A) A cFMS tyrosine kinase inhibitor, GW2580, rivals TMP-based stabilization in the eye and liver. Injected BALB/c mice (described in Figure 4) were administered 1 mg (50 mg/kg) GW2580 and imaged using bioluminescence. Mean fold change \pm SEM is shown. $n = 4-5$ mice; ** $p < 0.01$, *** $p < 0.001$, one-tailed t test versus control, untreated mice (shown in Figure 4).

(B) GW2580 can be used to simultaneously dampen Iba1(+) microglia/macrophage abundance in the eye and regulate ecDHFR.FLuc protein abundance.

Intravitreally injected BALB/c mice were dosed with 1 mg of GW2580 per day for 7 days via oral gavage, measured for bioluminescence (top panels), and sacrificed and evaluated for Iba1(+) microglia/macrophage in the inner retina (ganglion cell layer, middle panels) and outer retina (outer plexiform layer, bottom panels).

(C) Quantification of Iba1(+) cells in control versus mice treated with GW2580. Mean \pm SD, $n = 3-4$ mice; ** $p < 0.01$, two-way ANOVA versus control mice.

endogenous hsDHFR inhibition and HSF1 repression mediated through ecDHFR.dn-cHSF1 stabilization with aminopterin (100 nM, 1 μ M) or methotrexate (100 nM, 1 μ M) significantly compromised cell viability when compared with control cells (Figure 5C), indicating a synergistic effect of simultaneously inhibiting hsDHFR activity and HSF1 signaling.

Next, we evaluated whether a dual-function approach could also be used *in vivo*. We selected GW2580, a cFMS inhibitor that has received recent attention for its ability to repress microglia autocrine regulation in the central nervous system (Conway et al., 2005; Gerber et al., 2018; Olmos-Alonso et al., 2016), and paired it with an ocular-expressed ecDHFR.FLuc. Surprisingly, we found that GW2580 (1 mg, 50 mg/kg, 6 h, oral gavage) rivaled TMP in its ability to significantly stabilize an ocular ecDHFR DD (8.6 ± 1.7 fold); which is the first compound we have identified so far with TMP-like stabilization properties in the eye (Figure 6A). To determine whether this compound could repress microglia proliferation in the retina while simultaneously controlling an ecDHFR DD, we continued to gavage mice with GW2580 for 6 additional days. Indeed, a 7-day treatment of mice with GW2580 substantially stabilized ecDHFR.FLuc (Figure 6B) while significantly repressing Iba1(+) microglia in the eye (a reduction of 33% in the inner retina and 32% in the outer retina, Figures 6B and 6C). These results support the use of our newly identified stabilizers for simultaneously and conditionally controlling intricate endogenous and user-defined signaling pathways both *in vitro* and *in vivo*.

DISCUSSION

The work that we describe here significantly expands the small-molecule pharmacological space that can be utilized for regulating protein abundance through an ecDHFR DD. Previously, only TMP and 14a, a TMP derivative (Peng et al., 2019), were demonstrated to stabilize the ecDHFR DD *in vitro* and *in vivo*. Our studies verified 17 stabilizers, most of which were non-antibiotics incapable of suppressing *E. coli* and *S. aureus* growth, and many of which we confirmed *in vivo* in the eye and liver. While stabilization of the ecDHFR DD requires a specific pharmacophore (2,4-DAP/triazine connected to an aryl group), it is clear by the diversity of the active stabilizers (Figure S2) that

there is significant flexibility within the ecDHFR dihydrofolate binding pocket to accommodate the aryl group and additional modifications connected to the aryl ring structure. Thus, we identified not only previously characterized DHFR inhibitors (e.g., ormetoprim, methotrexate, pyrimethamine) but also unique molecules with formerly unknown/unclear DHFR-binding abilities (e.g., triamterene, GW2580, TC-P 262). These results are exciting in that they suggest that more compounds exist that could be leveraged for regulation of the ecDHFR DD system. Many of these compounds may exist in the virtual screen that we performed that includes 129 additional untested molecules (Table S1), some of which may stabilize ecDHFR DDs *in vivo* similarly to TMP, as we discovered with GW2580.

Our findings open two main routes of scientific pursuit. The first route is to employ these newly identified molecules to achieve simultaneous control of user-defined, ecDHFR DD-based genetic pathways combined with targeting of endogenous, compound-defined pathways. Based on the small molecules we have identified, which have been used for pain management (TC-P 262, a P2X₂/P2X_{2/3} antagonist), stem cell reprogramming (triamterene/epiblastin A, casein kinase 1 inhibitors [Illlich et al., 2016; Ursu et al., 2016]), microglia-based inflammation (GW2580, a cFMS kinase inhibitor), vascular permeability (TG100-115, a PI3K inhibitor), Gaucher disease (7,8-DQ-2,4-DA, a glucocerebrosidase pharmacological chaperone), or even hepatitis C (HZ-1157, a hepatitis C NS3/4A protease inhibitor), the potential for dual regulation appears to cover vast scientific interests. Moreover, many of the molecules that we have identified have been used in clinical trials (clinicaltrials.gov) for diverse conditions ranging from cancer (hsDHFR inhibitors methotrexate, aminopterin, and methotrexate) to rheumatoid arthritis (methotrexate) to myocardial infarction (TG100-115), and proteinuric kidney disease (triamterene), which increases the likelihood of safely using them *in vivo*.

There is an inherent challenge in utilizing the identified small molecules for dual use *in vivo*. One limitation is the ability to match the compound concentration required for adequate stabilization of the ecDHFR DD in parallel with a physiologically relevant concentration of the compound for targeting endogenous signaling. For example, HZ-1157 has an AC₅₀ >10 μ M

with respect to ecDHFR.YFP stabilization, whereas its IC₅₀ against hepatitis C virus NS3/4A protease is 1 μM (Yu et al., 2014). Thus, the concentrations required for the individual functions at 50% maximal response are disparate. Elevating the amount of compound used *in vivo* for controlling endogenous signaling will likely alter the specificity of the compound for the primary target. This phenomenon will have to be considered and evaluated on a case-by-case basis for each stabilizer.

The second route of scientific pursuit originating from these studies (as well as from our previous findings [Peng et al., 2019]) is the rational development of effective, custom-made small molecules that have a TMP-like stabilizing pharmacophore connected to a separate moiety that functions independently on endogenous signaling pathways. We feel that our work is not a comprehensive amalgamation of all the possible stabilizers, but rather the beginning of a realization that additional molecules can be developed or used as surrogates for TMP in this ecDHFR DD system. Based on the *in vitro* and *in vivo* effectiveness of 14a (Peng et al., 2019) and GW2580 toward stabilizing ecDHFR DDs, the TMP backbone at the 4' position of its benzyl ring appears to be a favorable site for modification that retains ecDHFR-binding capabilities but compromises the compound's antibiotic effectiveness. Ultimately, as our database of ecDHFR DD stabilizers increases, it may be possible to "mix and match" small-molecule stabilizers with defined functions, e.g., anti-inflammatory or antioxidant alongside validated ecDHFR DDs that control any number of pathways ranging from growth factor signaling (Quintino et al., 2018), to the unfolded protein response (Shoulders et al., 2013), to the heat-shock response (Moore et al., 2016), or even gene editing (Maji et al., 2017). These possible combinations will further expand the utility of the ecDHFR DD system and allow it to be utilized in increasingly complex biological and disease-related contexts in a manner that was previously unachievable.

SIGNIFICANCE

We demonstrate that stabilization of the ecDHFR DD can be achieved by a diverse set of molecules other than TMP, which contain a 2,4-diaminopyrimidine/triazine ring and an additional aryl group. Many of the compounds we identified can serve as unique ecDHFR DD stabilizers both *in vitro* and *in vivo* while not substantially affecting bacterial growth or hsDHFR activity. In fact, select compounds, such as GW2580, rival the *in vivo* stabilizing properties of TMP while also concomitantly repressing inflammation/microglia. Expansion of the chemical space able to stabilize the ecDHFR DD reveals the possibility of "chemical timers"—a diverse set of molecules that can achieve similar degrees of ecDHFR DD stabilization (amplitude), but do so with different kinetics—some with shorter windows (i.e., diaveridine) and some with longer windows (i.e., hsDHFR inhibitors). Such tools could be used to probe biology with increasing temporal flexibility. Additionally, our studies establish the minimum chemical properties required for stabilization of the ecDHFR DD and, in doing so, lay the foundation for the generation of rationally designed, custom-made stabilizers of this domain. Such stabilizers have the ability to simultaneously control compound-specific endogenous and user-

defined genetic pathways, the combination of which may provide synergistic effects in complex biological scenarios in which the ecDHFR DD has been used (e.g., biological probes of stress responses to gene editing to gene therapy).

STAR★METHODS

Detailed methods are provided in the online version of this paper and include the following:

- KEY RESOURCES TABLE
- LEAD CONTACT AND MATERIALS AVAILABILITY
- EXPERIMENTAL MODEL AND SUBJECT DETAILS
 - Cell Culture
 - Bacterial Growth Assays
 - Mouse Use
- METHOD DETAILS
 - High Content Screening
 - Virtual Compound Screen, ecDHFR DD Modeling and Docking Studies
 - Celigo/Western Blotting Confirmatory Assays
 - Human DHFR (hsDHFR) Inhibition Secondary Assay
 - Intravitreal Injections
 - Intravenous Tail Vein Injection
 - Oral Gavage
 - Bioluminescence Imaging
 - Immunohistochemical Analyses of Microglia in Retinal Flat-Mounts
- QUANTIFICATION AND STATISTICAL ANALYSIS
- DATA AND CODE AVAILABILITY

SUPPLEMENTAL INFORMATION

Supplemental Information can be found online at <https://doi.org/10.1016/j.chembiol.2020.03.006>.

ACKNOWLEDGMENTS

V.Q.C. was supported by funding from the UT Southwestern Summer Medical Student Research Program. J.D.H. is supported by an endowment from the Roger and Dorothy Hiril Research Fund, a vision research grant from the Karl Kirchgessner Foundation, a National Eye Institute (NEI) R21 grant (EY028261), an NEI R01 grant (EY027785), and a Career Development Award from RPB. Additional support was provided by an NEI Visual Science Core grant (P30 EY030413) and an unrestricted grant from RPB (both to the UT Southwestern Department of Ophthalmology). This project was supported by an NIH Shared Instrumentation S10 grant for the InCell Analyzer 6000 (ODO018005-01 to B.A.P.), and screening costs were subsidized by the Simmons National Cancer Institute-funded Cancer Center Support grant (5P30 CA 142543-03) and UT Southwestern. M.M. and P.M.D. are supported by the Welch Foundation (I-1920-20170325), a National Institute on Aging (NIA) R01 grant (AG061338), a CPRIT grant (RR150089), and the Harmon Center for Regenerative Science and Medicine (UT Southwestern).

We thank Khiem T. Vu, MD for initial generation of the ARPE-19 R12Y/G67S/Y100I ecDHFR.YFP cell line. We thank Erdal Toprak, PhD (UT Southwestern) for access to the Tecan robot, Matthew E.R. Butchbach, PhD (University of Delaware) for providing RG3039 and D156844 for testing, and Matthew D. Shoulders, PhD (Massachusetts Institute of Technology) for providing the pLenti CMV puro dn.c-HSF1 plasmid.

AUTHOR CONTRIBUTIONS

Conceptualization, J.D.H.; Investigation, P.R., D.R.W., S.D., H.P., P.L.M., H.N., M.M., V.Q.C., and J.D.H.; Writing – Original Draft, P.R. and J.D.H.;

Writing – Review & Editing, P.R., D.R.W., S.D., H.P., P.L.M., H.N., M.M., V.Q.C., P.M.D., B.A.P., and J.D.H.; Funding Acquisition, P.M.D., B.A.P., and J.D.H.; Supervision, P.M.D., B.A.P., and J.D.H.

DECLARATION OF INTERESTS

The authors declare no competing interests.

Received: December 11, 2019

Revised: February 4, 2020

Accepted: March 6, 2020

Published: April 23, 2020

REFERENCES

- Baim, A.D., Movahedan, A., Farooq, A.V., and Skondra, D. (2019). The microbiome and ophthalmic disease. *Exp. Biol. Med. (Maywood)* *244*, 419–429.
- Ballini, E., Virginio, C., Medhurst, S.J., Summerfield, S.G., Aldegheri, L., Buson, A., Carignani, C., Chen, Y.H., Giacometti, A., Lago, I., et al. (2011). Characterization of three diaminopyrimidines as potent and selective antagonists of P2X3 and P2X2/3 receptors with in vivo efficacy in a pain model. *Br. J. Pharmacol.* *163*, 1315–1325.
- Banaszynski, L.A., Chen, L.-c., Maynard-Smith, L.A., Ooi, A.G.L., and Wandless, T.J. (2006). A rapid, reversible, and tunable method to regulate protein function in living cells using synthetic small molecules. *Cell* *126*, 995–1004.
- Boehr, D.D., McElheny, D., Dyson, H.J., and Wright, P.E. (2006). The dynamic energy landscape of dihydrofolate reductase catalysis. *Science* *313*, 1638–1642.
- Butchbach, M.E., Singh, J., Thorsteinsdottir, M., Saieva, L., Slominski, E., Thurmond, J., Andresson, T., Zhang, J., Edwards, J.D., Simard, L.R., et al. (2010). Effects of 2,4-diaminoquinazoline derivatives on SMN expression and phenotype in a mouse model for spinal muscular atrophy. *Hum. Mol. Genet.* *19*, 454–467.
- Cao, H., Gao, M., Zhou, H., and Skolnick, J. (2018). The crystal structure of a tetrahydrofolate-bound dihydrofolate reductase reveals the origin of slow product release. *Commun. Biol.* *1*, 226.
- Carroll, M.J., Mauldin, R.V., Gromova, A.V., Singleton, S.F., Collins, E.J., and Lee, A.L. (2012). Evidence for dynamics in proteins as a mechanism for ligand dissociation. *Nat. Chem. Biol.* *8*, 246–252.
- Chen, J.J., Geneux, J.C., Qu, S., Hulleman, J.D., Shoulders, M.D., and Wiseman, R.L. (2014). ATF6 activation reduces the secretion and extracellular aggregation of destabilized variants of an amyloidogenic protein. *Chem. Biol.* *21*, 1564–1574.
- Chunduru, S.K., Cody, V., Luft, J.R., Pangborn, W., Appleman, J.R., and Blakley, R.L. (1994). Methotrexate-resistant variants of human dihydrofolate reductase. Effects of Phe31 substitutions. *J. Biol. Chem.* *269*, 9547–9555.
- Conway, J.G., McDonald, B., Parham, J., Keith, B., Rusnak, D.W., Shaw, E., Jansen, M., Lin, P., Payne, A., Crosby, R.M., et al. (2005). Inhibition of colony-stimulating-factor-1 signaling in vivo with the orally bioavailable cFMS kinase inhibitor GW2580. *Proc. Natl. Acad. Sci. U S A* *102*, 16078–16083.
- Cooley, C.B., Ryno, L.M., Plate, L., Morgan, G.J., Hulleman, J.D., Kelly, J.W., and Wiseman, R.L. (2014). Unfolded protein response activation reduces secretion and extracellular aggregation of amyloidogenic immunoglobulin light chain. *Proc. Natl. Acad. Sci. U S A* *111*, 13046–13051.
- Corcino, J., Waxman, S., and Herbert, V. (1970). Mechanism of triamterene-induced megaloblastosis. *Ann. Intern. Med.* *73*, 419–424.
- Crosley, A.P., Jr., Ronquillo, L.M., Strickland, W.H., and Alexander, F. (1962). Triamterene, a new natriuretic agent. Preliminary observations in man. *Ann. Intern. Med.* *56*, 241–251.
- Dai, C., and Sampson, S.B. (2016). HSF1: guardian of proteostasis in cancer. *Trends Cell Biol.* *26*, 17–28.
- Datta, S., Renwick, M., Chau, V.Q., Zhang, F., Nettesheim, E.R., Lipinski, D.M., and Hulleman, J.D. (2018). A destabilizing domain allows for fast, noninvasive, conditional control of protein abundance in the mouse eye—implications for ocular gene therapy. *Invest. Ophthalmol. Vis. Sci.* *59*, 4909–4920.
- Datta, S., Peng, H., and Hulleman, J.D. (2019). Small molecule-based inducible gene therapies for retinal degeneration. *Adv. Exp. Med. Biol.* *1185*, 65–69.
- DeGraw, J.I., Colwell, W.T., Piper, J.R., and Sirotnak, F.M. (1993). Synthesis and antitumor activity of 10-propargyl-10-deazaaminopterin. *J. Med. Chem.* *36*, 2228–2231.
- Dias, M.V., Tyrakis, P., Domingues, R.R., Paes Leme, A.F., and Blundell, T.L. (2014). Mycobacterium tuberculosis dihydrofolate reductase reveals two conformational states and a possible low affinity mechanism to antifolate drugs. *Structure* *22*, 94–103.
- Doukas, J., Wrasidlo, W., Noronha, G., Dneprovskaja, E., Fine, R., Weis, S., Hood, J., Demaria, A., Soll, R., and Cheresch, D. (2006). Phosphoinositide 3-kinase gamma/delta inhibition limits infarct size after myocardial ischemia/reperfusion injury. *Proc. Natl. Acad. Sci. U S A* *103*, 19866–19871.
- Gerber, Y.N., Saint-Martin, G.P., Bringuier, C.M., Bartolami, S., Goze-Bac, C., Noristani, H.N., and Perrin, F.E. (2018). CSF1R inhibition reduces microglia proliferation, promotes tissue preservation and improves motor recovery after spinal cord injury. *Front. Cell. Neurosci.* *12*, 368.
- Harris, A.W., and Butchbach, M.E. (2015). The effect of the DcpS inhibitor D156844 on the protective action of follistatin in mice with spinal muscular atrophy. *Neuromuscul. Disord.* *25*, 699–705.
- Horai, R., and Caspi, R.R. (2019). Microbiome and autoimmune uveitis. *Front. Immunol.* *10*, 232.
- Illich, D.J., Zhang, M., Ursu, A., Osorno, R., Kim, K.P., Yoon, J., Arauzo-Bravo, M.J., Wu, G., Esch, D., Sabour, D., et al. (2016). Distinct signaling requirements for the establishment of ESC pluripotency in late-stage EpiSCs. *Cell Rep.* *15*, 787–800.
- Iwamoto, M., Bjorklund, T., Lundberg, C., Kirik, D., and Wandless, T.J. (2010). A general chemical method to regulate protein stability in the mammalian central nervous system. *Chem. Biol.* *17*, 981–988.
- Jaswant, S., Misra, B.G., Ray, A.P., Basu, P.C., and Bami, H.L. (1951). Daraprim (50-63) in simian malaria. *Indian J. Malariol.* *5*, 531–540.
- Kho, Z.Y., and Lal, S.K. (2018). The human gut microbiome—a potential controller of wellness and disease. *Front. Microbiol.* *9*, 1835.
- Lee, J., Yennawar, N.H., Gam, J., and Benkovic, S.J. (2010). Kinetic and structural characterization of dihydrofolate reductase from *Streptococcus pneumoniae*. *Biochemistry* *49*, 195–206.
- Li, R., Sirawaraporn, R., Chitnumsub, P., Sirawaraporn, W., Wooden, J., Athappilly, F., Turley, S., and Hol, W.G. (2000). Three-dimensional structure of *M. tuberculosis* dihydrofolate reductase reveals opportunities for the design of novel tuberculosis drugs. *J. Mol. Biol.* *295*, 307–323.
- Maji, B., Moore, C.L., Zetsche, B., Volz, S.E., Zhang, F., Shoulders, M.D., and Choudhary, A. (2017). Multidimensional chemical control of CRISPR-Cas9. *Nat. Chem. Biol.* *13*, 9–11.
- Manna, D., Maji, B., Gangopadhyay, S.A., Cox, K.J., Zhou, Q., Law, B.K., Mazitschek, R., and Choudhary, A. (2019). A singular system with precise dosing and spatiotemporal control of CRISPR-Cas9. *Angew. Chem. Int. Ed.* *58*, 6285–6289.
- Mauldin, R.V., Sapienza, P.J., Petit, C.M., and Lee, A.L. (2012). Structure and dynamics of the G121V dihydrofolate reductase mutant: lessons from a transition-state inhibitor complex. *PLoS One* *7*, e33252.
- Miyazaki, Y., Imoto, H., Chen, L.C., and Wandless, T.J. (2012). Destabilizing domains derived from the human estrogen receptor. *J. Am. Chem. Soc.* *134*, 3942–3945.
- Moore, C.L., Dewal, M.B., Nekongo, E.E., Santiago, S., Lu, N.B., Levine, S.S., and Shoulders, M.D. (2016). Transportable, chemical genetic methodology for the small molecule-mediated inhibition of heat shock factor 1. *ACS Chem. Biol.* *11*, 200–210.
- Olmos-Alonso, A., Schettters, S.T., Sri, S., Askew, K., Mancuso, R., Vargas-Caballero, M., Holscher, C., Perry, V.H., and Gomez-Nicola, D. (2016). Pharmacological targeting of CSF1R inhibits microglial proliferation and prevents the progression of Alzheimer’s-like pathology. *Brain* *139*, 891–907.
- Peng, H., Chau, V.Q., Phetsang, W., Sebastian, R.M., Stone, M.R.L., Datta, S., Renwick, M., Tamer, Y.T., Toprak, E., Koh, A.Y., et al. (2019). Non-antibiotic

- small-molecule regulation of DHFR-based destabilizing domains *in vivo*. *Mol. Ther. Methods Clin. Dev.* **15**, 27–39.
- Quintino, L., Manfre, G., Wettergren, E.E., Namislo, A., Isaksson, C., and Lundberg, C. (2013). Functional neuroprotection and efficient regulation of GDNF using destabilizing domains in a rodent model of Parkinson's disease. *Mol. Ther.* **21**, 2169–2180.
- Quintino, L., Namislo, A., Davidsson, M., Breger, L.S., Kavanagh, P., Avallone, M., Elgstrand-Wettergren, E., Isaksson, C., and Lundberg, C. (2018). Destabilizing domains enable long-term and inert regulation of GDNF expression in the brain. *Mol. Ther. Methods Clin. Dev.* **11**, 29–39.
- Raimondi, M.V., Randazzo, O., La Franca, M., Barone, G., Vignoni, E., Rossi, D., and Collina, S. (2019). DHFR inhibitors: reading the past for discovering novel anticancer agents. *Molecules* **24**, <https://doi.org/10.3390/molecules24061140>.
- Ravkin, I., and Temov, V. (1988). Bit representation techniques and image processing. *Appl. Inform.* **14**, 41–90.
- Reid, C.A., Ertel, K.J., and Lipinski, D.M. (2017). Improvement of photoreceptor targeting via intravitreal delivery in mouse and human retina using combinatory rAAV2 capsid mutant vectors. *Invest. Ophthalmol. Vis. Sci.* **58**, 6429–6439.
- Reisberg, B., Herzog, J., and Weinstein, L. (1966). *In vitro* antibacterial activity of trimethoprim alone and combined with sulfonamides. *Antimicrob. Agents Chemother.* (Bethesda) **6**, 424–429.
- Ryno, L.M., Genereux, J.C., Naito, T., Morimoto, R.I., Powers, E.T., Shoulders, M.D., and Wiseman, R.L. (2014). Characterizing the altered cellular proteome induced by the stress-independent activation of heat shock factor 1. *ACS Chem. Biol.* **9**, 1273–1283.
- Sando, R., 3rd, Baumgaertel, K., Pieraut, S., Torabi-Rander, N., Wandless, T.J., Mayford, M., and Maximov, A. (2013). Inducible control of gene expression with destabilized Cre. *Nat. Methods* **10**, 1085–1088.
- Santagata, S., Hu, R., Lin, N.U., Mendillo, M.L., Collins, L.C., Hankinson, S.E., Schnitt, S.J., Whitesell, L., Tamimi, R.M., Lindquist, S., et al. (2011). High levels of nuclear heat-shock factor 1 (HSF1) are associated with poor prognosis in breast cancer. *Proc. Natl. Acad. Sci. U S A* **108**, 18378–18383.
- Sastry, G.M., Adzhigirey, M., Day, T., Annabhimoju, R., and Sherman, W. (2013). Protein and ligand preparation: parameters, protocols, and influence on virtual screening enrichments. *J. Comput. Aided Mol. Des.* **27**, 221–234.
- Sawaya, M.R., and Kraut, J. (1997). Loop and subdomain movements in the mechanism of *Escherichia coli* dihydrofolate reductase: crystallographic evidence. *Biochemistry* **36**, 586–603.
- Shoulders, M.D., Ryno, L.M., Genereux, J.C., Moresco, J.J., Tu, P.G., Wu, C., Yates, J.R., 3rd, Su, A.I., Kelly, J.W., and Wiseman, R.L. (2013). Stress-independent activation of XBP1s and/or ATF6 reveals three functionally diverse ER proteostasis environments. *Cell Rep.* **3**, 1279–1292.
- Tai, K., Quintino, L., Isaksson, C., Gussing, F., and Lundberg, C. (2012). Destabilizing domains mediate reversible transgene expression in the brain. *PLoS One* **7**, e46269.
- Tamer, Y.T., Gaszek, I.K., Abdizadeh, H., Batur, T.A., Reynolds, K., Atilgan, A.R., Atilgan, C., and Toprak, E. (2019). High-order epistasis in catalytic power of dihydrofolate reductase gives rise to a rugged fitness landscape in the presence of trimethoprim selection. *Mol. Biol. Evol.* **36**, 1533–1550.
- Toprak, E., Veres, A., Michel, J.B., Chait, R., Hartl, D.L., and Kishony, R. (2011). Evolutionary paths to antibiotic resistance under dynamically sustained drug selection. *Nat. Genet.* **44**, 101–105.
- Tropak, M.B., Kornhaber, G.J., Rigat, B.A., Maegawa, G.H., Buttner, J.D., Blanchard, J.E., Murphy, C., Tuske, S.J., Coales, S.J., Hamuro, Y., et al. (2008). Identification of pharmacological chaperones for Gaucher disease and characterization of their effects on beta-glucocerebrosidase by hydrogen/deuterium exchange mass spectrometry. *Chembiochem* **9**, 2650–2662.
- Ursu, A., Illich, D.J., Takemoto, Y., Porfetye, A.T., Zhang, M., Brockmeyer, A., Janning, P., Watanabe, N., Osada, H., Vetter, I.R., et al. (2016). Epiblastin A induces reprogramming of epiblast stem cells into embryonic stem cells by inhibition of casein kinase 1. *Cell Chem. Biol.* **23**, 494–507.
- Vu, K.T., and Hulleman, J.D. (2017). An inducible form of Nrf2 confers enhanced protection against acute oxidative stresses in RPE cells. *Exp. Eye Res.* **164**, 31–36.
- Vu, K.T., Zhang, F., and Hulleman, J.D. (2017). Conditional, genetically encoded, small molecule-regulated inhibition of NFkappaB signaling in RPE cells. *Invest. Ophthalmol. Vis. Sci.* **58**, 4126–4137.
- Yu, Y., Jing, J.F., Tong, X.K., He, P.L., Li, Y.C., Hu, Y.H., Tang, W., and Zuo, J.P. (2014). Discovering novel anti-HCV compounds with inhibitory activities toward HCV NS3/4A protease. *Acta Pharmacol. Sin.* **35**, 1074–1081.

STAR★METHODS

KEY RESOURCES TABLE

REAGENT or RESOURCE	SOURCE	IDENTIFIER
Antibodies		
HA Tag Mouse Monoclonal Antibody (2-2.2.14)	Invitrogen	Cat#26183
β-Actin Rabbit Monoclonal Antibody	LI-COR	Cat# P/N 926-42210
HSF1 Antibody #4356	Cell Signaling	Cat# 4356T
Anti-Iba1, Rabbit (for Immunocytochemistry)	FujiFilm Wako Chemicals	Cat# 019-19741
Goat anti-Rabbit IgG (H+L) Cross-Adsorbed Secondary Antibody, Alexa Fluor 488	Invitrogen	Cat# A-11008
IRDye® 680RD Goat anti-Mouse IgG Secondary Antibody	LI-COR	Cat# P/N: 926-68070
IRDye® 800CW Goat anti-Rabbit IgG Secondary Antibody	LI-COR	Cat# P/N: 926-32211
Bacterial and Virus Strains		
Lentivirus: R12Y/G67S/Y100I ecDHFR.YFP.HA	This paper	N/A
Lentivirus: I5F/R12Y/G67S/Y100I ecDHFR.YFP.HA	This paper	N/A
Lentivirus: R12Y/M16L/G67S/Y100I ecDHFR.YFP.HA	This paper	N/A
Lentivirus: R12Y/F31L/G67S/Y100I ecDHFR.YFP.HA	This paper	N/A
Lentivirus: R12Y/G67S/I94L/Y100I ecDHFR.YFP.HA	This paper	N/A
Lentivirus: ecDHFR.dn-cHSF1	This paper	N/A
AAV Virus: AAV2/2 MAX NanoLuc 2A ecDHFR FLuc	Packaged by UNC Viral Vector Core	N/A
AAV Virus: AAV2/8 NanoLuc 2A ecDHFR.Fluc	Packaged by UNC Viral Vector Core	N/A
Bacteria: wild-type <i>S. aureus</i>	Marrafini Laboratory, Rockefeller University	RN4220
Bacteria: wild-type <i>E. coli</i>	Toprak Laboratory, UT Southwestern	BW25113
Chemicals, Peptides, and Recombinant Proteins		
Dimethyl Sulfoxide (DMSO)	Fisher Scientific	Cat# BP231-100
Carbowax™ PEG 400 (NF)	Fisher Scientific	Cat# P167-1
Tween™ 80	Fisher Scientific	Cat# BP338-500
Tween™ 20	Fisher Scientific	Cat# BP337-100
Cremophor EL	Millipore Sigma	Cat# 238470
Dextrose Anhydrous (Crystalline Granules/Molecular Biology)	Fisher Scientific	Cat# BP350-500
HBSS	Sigma	Cat# H6648
D-Luciferin Sodium Salt	Gold Biotechnology	Cat# LUCNA
0.9% Sodium Chloride Injection, USP	Hospira	N/A
Ponceau S solution	Sigma	Cat# P7170
2-aminoquinazoline	Sigma	Cat# CDS008332
2-amino-3H-quinazolin-4-one	Sigma	Cat# CDS020257
2,4-diaminopyrimidine	Sigma	Cat# 68231
2,4-diaminopyrimidine-5-carbaldehyde	Sigma	Cat# CDS013913
Dihydrofolic acid	Sigma	Cat# D7006
pemetrexed	Tocris Bioscience	Cat# 6185
Proguanil HCl	Acros Organics	Cat# 637-32-1
raltitrexed	Apex Bioscience	Cat# B1476
RG3039	Butchbach Laboratory, University of Delaware	N/A

(Continued on next page)

Continued

REAGENT or RESOURCE	SOURCE	IDENTIFIER
D156844	Butchbach Laboratory, University of Delaware	N/A
Trimethoprim	Sigma	Cat# T7883
Methotrexate	Fisher Scientific	Cat# BP2665
Triamterene	Selleck Chemicals	Cat# S4080
Ormetoprim, 98%	J&K	Cat# 403370
Pyrimethamine	Tocris Bioscience	Cat# 3918
SW000198-2	ChemDiv	Cat# 0075-0058
Pralatrexate	Apex Bio	Cat# A4350
Diaveridine	Santa Cruz	Cat# SC-205646
Aminopterin	Sigma	Cat# A3411
Cycloguanil	Cayman Chemical	Cat# 16861
2,4-diaminoquinazoline	Alfa Aesar	Cat# L13783
WR99210	Sigma	Cat# W1770
GW2580	Apex Bio	Cat# A1655
TC-P 262	Tocris Bioscience	Cat# 4386
Epiblastin A	Sigma	Cat# SML1647
TG100-115	Selleck Chemicals	Cat# S1352
7,8-DIETHOXY-QUINAZOLINE-2,4-DIAMINE	Sigma	Cat# R396540
HZ-1157	ACheckBlock	Cat# O33918
Critical Commercial Assays		
Pierce™ BCA Protein Assay Kit	ThermoFisher Scientific	Cat# 23227
Dihydrofolate Reductase Assay Kit	Sigma	Cat# CS0340
Maxi Prep Plus Kit	Qiagen	Cat# 12943
Deposited Data		
<i>E. coli</i> DHFR substrate complex with dihydrofolate	Cao et al., 2018	PDB ID: 6CXK
<i>E. coli</i> DHFR complex with methotrexate	Sawaya and Kraut, 1997	PDB ID: 1RA3
<i>M. tuberculosis</i> DHFR in complex with cycloguanil	Dias et al., 2014	PDB ID: 4KNE
Experimental Models: Cell Lines		
Human: HEK-293A	Life Technologies	Cat# R70507
Human: HeLa Tet-On	Takara	Cat# 631183
Human: ARPE-19	American Type Culture Collection	Cat# CRL-2302
ARPE-19 R12Y/G67S/Y100I ecDHFR.YFP.HA	This paper	N/A
ARPE-19 I5F/R12Y/G67S/Y100I ecDHFR.YFP.HA	This paper	N/A
ARPE-19 R12Y/M16L/G67S/Y100I ecDHFR.YFP.HA	This paper	N/A
ARPE-19 R12Y/F31L/G67S/Y100I ecDHFR.YFP.HA	This paper	N/A
ARPE-19 R12Y/G67S/I94L/Y100I ecDHFR.YFP.HA	This paper	N/A
HeLa R12Y/G67S/Y100I ecDHFR.YFP.HA	This paper	N/A
HeLa ecDHFR.dn-cHSF1	This paper	N/A
Experimental Models: Organisms/Strains		
Mouse: Wild Type Balb/c	Jackson Laboratories, private stock courtesy of Lihua Marmorstein	N/A
Oligonucleotides		
Primer: I5F ecDHFR Forward 5' GATCAGTCTGTTTGC GGCGTTAG '3	Sigma	N/A
Primer: I5F ecDHFR Reverse 5' ATGGTGGCGGATCCAGTC '3	Sigma	N/A
Primer: I94L ecDHFR Forward 5' AATCATGGTGCTTGGCGGCGG '3	Sigma	N/A

(Continued on next page)

Continued

REAGENT or RESOURCE	SOURCE	IDENTIFIER
Primer: I94L ecDHFR Reverse 5' TCTGGTACGTCACCCACAC '3	Sigma	N/A
Primer: F31L ecDHFR Forward 5' TCGCCTGGTTAAAACGCAACAC '3	Sigma	N/A
Primer: F31L ecDHFR Reverse 5' GATCGGCAGGCAGGTTCC '3	Sigma	N/A
Primer: M16L ecDHFR Forward 5' CGTTATCGGCCTGGAAAACGC '3	Sigma	N/A
Primer: M16L ecDHFR Reverse 5' TAATCTACCGCTAACGCC '3	Sigma	N/A
Primer: CMV Forward Sequencing Primer 5' CCAAGTACGCCCTATTGA '3	Sigma	N/A
Recombinant DNA		
pAAV2/2 MAX (7m8, QuadYF)	Reid et al., 2017	N/A
pAAV2/8	Zhu Laboratory, UT Southwestern	N/A
pTR smCBA Nluc 2A ecDHFR Fluc	Peng et al., 2019	N/A
pLenti Puro R12Y/G67S/Y100I ecDHFR.YFP.HA	This paper	N/A
pLenti Puro I5F/R12Y/G67S/Y100I ecDHFR.YFP.HA	This paper	N/A
pLenti Puro R12Y/M16L/G67S/Y100I ecDHFR.YFP.HA	This paper	N/A
pLenti Puro R12Y/F31L/G67S/Y100I ecDHFR.YFP.HA	This paper	N/A
pLenti Puro R12Y/G67S/I94L/Y100I ecDHFR.YFP.HA	This paper	N/A
pLenti Puro ecDHFR-dn.cHSF1	Moore et al., 2016	N/A
Software and Algorithms		
GraphPad Prism	GraphPad Software, Inc	https://www.graphpad.com/scientific-software/prism/
CellProfiler 3.1.8	Broad Institute	https://cellprofiler.org/releases/
Protein Preparation Wizard	Schrodinger LLC	https://www.schrodinger.com/protein-preparation-wizard
Maestro v11.9.011	Schrodinger, LLC	https://www.schrodinger.com/maestro
SnapGene	GSL Biotech	https://www.snapgene.com/
Other		
National Cancer Institute (NCI) preclinical experimental collection	NCI	N/A
Prestwick Chemical Library	Prestwick Chemical	http://www.prestwickchemical.com/libraries-screening-lib-pcl.html
ad hoc portion of University of Texas Southwestern 300k collection	UT Southwestern	N/A
eMolecules Chemical Database	eMolecules, Inc.	https://www.emolecules.com/
MolPort Chemical Database	MolPort	https://www.molport.com/shop/index

LEAD CONTACT AND MATERIALS AVAILABILITY

Further information and requests for resources and reagents should be directed to and will be fulfilled by the Lead Contact, John D. Hulleman (john.hulleman@utsouthwestern.edu). All unique/stable reagents generated in this study are available from the Lead Contact without restriction.

EXPERIMENTAL MODEL AND SUBJECT DETAILS

Cell Culture

Human immortalized retinal pigmented epithelial cells (ARPE-19, male, CRL-2302, American Type Culture Collection, Manassas, VA) were cultured in DMEM/F12 media supplemented with 10% fetal bovine serum (FBS, Omega Scientific, Tarzana, CA), HEPES (Corning, Corning, NY) and penicillin/streptomycin and glutamine (PSQ, Gibco, Germantown, MD). Human embryonic kidney cells

(HEK-293A, female, R70507, Life Technologies, Carlsbad, CA) were cultured in DMEM high glucose media supplemented with 10% FBS and PSQ. Human cervical cancer cells (HeLa Tet-On, female, #631183, Takara, Kusatsu, Japan) were cultured in MEM media supplemented with 10% FBS and PSQ. ARPE-19 or HeLa Tet-On cells were infected with a vesicular stomatitis virus G-protein (VSV-G) pseudotyped lentivirus (generated as described previously (Vu and Hulleman, 2017), DNA purified using a Plasmid Plus Maxi Prep Kit, Qiagen, Germantown, MD) encoding for either *E. coli* dihydrofolate reductase (ecDHFR) containing three destabilizing mutations (R12Y/G67S/Y100I (Iwamoto et al., 2010)) followed by yellow fluorescent protein (YFP) and a hemagglutinin (HA) tag, a dominant negative version of human heat shock factor 1 (dn.cHSF1, described previously (Moore et al., 2016)), or ecDHFR.YFP containing an additional mutation (i.e., I5F, M16L, F31L, or I94L, generated by the Q5 Site-Directed Mutagenesis Kit [New England Biolabs, Ipswich, MA]). A stable, heterogenous cell population was then selected using puromycin (1–2 $\mu\text{g}/\text{mL}$) and expanded for use in high content screening and validation studies. Cell lines were verified by short tandem repeat profiling (STR, University of Arizona, Tucson, AZ).

Bacterial Growth Assays

BW25113 wild-type (WT) *E. coli* (with WT DHFR) were grown overnight in M9 minimal media (supplemented with 0.4% glucose and 0.2% ampicillin), followed by an optical density (OD_{600}) measurement using spectrophotometry. The overnight culture was diluted to 1×10^{-4} OD in M9 media and aliquoted into 100 μL volumes in a 96-well plate (Wuxi NEST, Jiangsu, China). TMP and the hit compounds (5–10 mM in DMSO) were diluted in M9 minimal media at 8 interval concentrations and were subsequently combined with culture aliquots at a 1:1 volume ratio (50 μM to 0.02 μM , final concentration). WT *S. aureus* (strain RN4220, courtesy of the Marrafini Laboratory, Rockefeller University) were grown overnight in Luria-Bertani (LB) broth and were diluted and plated as described above for *E. coli*, except in LB broth. We should note that LB broth contains reasonable levels of thymidine, which may antagonize antifolate activity of the assayed compounds. Plates were incubated in a 37°C shaker or using a temperature-controlled automated robot system (TECAN, Mannedorf, Switzerland). Bacterial density of each dilution was measured as a function of time and endpoint data (19–24 h) are presented. Growth curves were generated by curve-fitting normalized bacterial densities vs. compound concentrations (GraphPad Prism, San Diego, CA).

Mouse Use

All animal experiments followed the guidelines of the ARVO Statement for the Use of Animals in Ophthalmic and Vision Research and were approved by the Institutional Animal Care and Use Committee (IACUC) of UT Southwestern Medical Center, Dallas, TX. Wild-type Balb/c mice originated from heterozygous breeding schemes from R345W[±] EFEMP1 mice (courtesy of Lihua Marmorstein, private stock at Jackson Labs). Littermate, age-matched male and female mice were used whenever possible. Mice were kept in non-barrier, climate-controlled conditions under a 12 h light/dark cycle and given free access to food/water.

METHOD DETAILS

High Content Screening

Fifteen cm dishes were used to expand enough ARPE-19 ecDHFR.YFP cells for performing high content screening (~1 x 15 cm dish per 384 well screening plate). On day 0 of plating, cells were washed with Hanks buffered salt solution (HBSS, Sigma, St. Louis, MO) and trypsinized with 0.25% trypsin/EDTA (Gibco). Cells were spun at 1000 RPM for 5 min and resuspended in fresh media at a concentration of $\sim 1.66 \times 10^5$ cells/mL. Sixty microliters (~10,000 cells) of cell suspension was dispensed into 384 well plates (Greiner) using a MultiFlo reagent dispenser (BioTek, Winooski, VT). Plates were then incubated overnight at 37°C to attach. Cells were subsequently treated with either DMSO (vehicle), trimethoprim (TMP, positive control), the proteasome inhibitor, MG132 (a false positive), or 5 μM screening compound using an Echo555 (Labcyte, San Jose, CA). The following libraries were screened: the National Cancer Institute (NCI) preclinical experimental collection [446 compounds], the Prestwick Chemical Library [1280 off-patent, approved drugs], and an ad-hoc set of the UT Southwestern 300k collection [1858 compounds]. Cells were treated for 24 h followed by extensive washing in Dulbecco's phosphate buffered saline (DPBS) and fixation in 4% formalin (Fisher Scientific, Waltham, MA). After fixation, Hoechst (1 $\mu\text{g}/\text{mL}$) was added to visualize cell nuclei. Individual wells were imaged using a General Electric (GE) IN Cell Analyzer 6000 at 10x magnification and 4 fields of view/well. Images were analyzed using CellProfiler 3.1.8 to quantify total YFP intensity and granularity. Specifically, granularity measurements were performed with CellProfiler 3.1.8 using the default size settings on the module. With this module, a size series of structural elements are programmatically fitted into the image. The output is a spectrum of measures that describe the quality of the fit for the structural elements to the intensity distribution of the tested image. In the comparison between control (TMP) smooth and granular (DMSO or MG132-treated) ecDHFR.YFP images, only the first component of the spectrum was informative and discriminating. This value was used for scoring granularity activity during the screening process (Ravkin and Temov, 1988). Nuclear count was measured to account for potential compound toxicity. Hit compounds were defined as having an intensity of ≥ 3 standard deviations of all the compounds in each respective plate. Potential false positives were excluded by high granularity scores (see MG132, for example in Figures 1D and 1E). The compound hit list was further culled by increasing the stringency of the YFP intensity value to $\geq 20\%$ of the control TMP value and having $\geq 35\%$ reduced granularity when compared to DMSO-treated cells. Thus, a true hit compound would not only increase YFP intensity, but also reduce basal YFP granularity. Hit compounds were then screened in a dose-response assay beginning at 1 nM to 10 μM using a $\frac{1}{2}$ log scale.

Virtual Compound Screen, ecDHFR DD Modeling and Docking Studies

Molport (<https://www.molport.com/>) and eMolecule (<https://reaxys.emolecules.com/>) databases were searched for compounds containing the 2,4-diaminopyrimidine substructure combined with an aryl group extending from the 1 or 6 position in the pyrimidine ring. For modeling/docking experiments, the crystal structure of ecDHFR (PDB ID: 6CXK) (Cao et al., 2018) co-crystalized with dihydrofolate (1.1 Å resolution) was obtained from the Protein Data Bank ([rcsb.org](https://www.rcsb.org/)). The R12Y, G67S, and Y100I mutations were made using the 'Protein Builder' module in MOE v2018.01 (Chemical Computing Group, Montreal, Canada). The sidechain of each mutant residue was allowed to relax via energy minimization while keeping the rest of the protein structure fixed. The triple mutant ecDHFR, which is an N-terminal destabilizing domain, was subsequently optimized using Protein Preparation Wizard (Schrodinger LLC, New York, New York) (Sastry et al., 2013). The optimization method included addition of hydrogens and step-wise energy minimization using an OPLS3e force field. Docking studies were performed using the model described above for the triple mutant ecDHFR model with dihydrofolate (Cao et al., 2018). Dihydrofolate was used as a reference to define a grid box for docking analysis. 2,4-diaminoquinoline (2,4-DAQ), 2-aminoquinolizine (2-AQ), and 2,4-diaminopyrimidine (2,4-DAP) 3D conformations were docked using the SP scoring function in Glide (Schrodinger LLC). Docking was performed by keeping the protein rigid while the ligands were allowed to be flexible. Docking results were analyzed visually using Maestro v11.9.011 release 2019-1 (Schrodinger LLC) and MOE v2018.01.

Celigo/Western Blotting Confirmatory Assays

As a secondary assay to confirm protein stabilization and to eliminate hits that were false positives due to autofluorescence, we validated a series of hit compounds using plate-based imaging and western blotting. ARPE-19 ecDHFR.YFP cells were plated at a density of 7,500 - 30,000 cells/well in clear-bottom 96 well plates (Corning) and allowed to attach overnight. Cells were then treated with the indicated compounds for 24 h followed by imaging and quantitation using a Celigo imaging cytometer (Nexcelom, Lawrence, MA). For dynamic stabilization/destabilization experiments, cells were treated and then imaged 2, 4, 6, 8, or 24 h later (designated as "On") followed by removal of cell culture media, a wash with HBSS and addition of fresh media. Cells were again imaged 2, 4, 6, 8, 24 and 48 h post media change (designated as "Off"). For western blotting, cells were lysed in each well using radioimmunoprecipitation assay (RIPA) buffer (Santa Cruz, Dallas, TX) supplemented with protease inhibitors (Pierce, Rockford, IL) and benzonase (Sigma, St. Louis, MO). Soluble protein (1-12 µg) was then assayed for protein content using a bicinchoninic acid (BCA) assay (Pierce), normalized, and run on a reducing 4-20% Tris-Glyc SDS-PAGE gel (Life Technologies). Proteins were transferred to nitrocellulose membranes using an iBlot2 (Life Technologies), stained for total protein using Ponceau S (Sigma), and blocked overnight using PBS blocking buffer (LI-COR, Lincoln, NE). Membranes were then probed using anti-HA (1:1500, clone 2-2.2.14, Pierce), anti-β actin (1:1400, #926-42210, LI-COR), or anti-HSF1 (1:1000, ADI-SPA-901, Enzo Life Sciences, Farmingdale, NY) for 1 h at RT followed by appropriate near-IR secondary antibodies (LI-COR) for 40 min at RT. Blots were imaged on an Odyssey CLx and quantified using Image Studio software (LI-COR).

Human DHFR (hsDHFR) Inhibition Secondary Assay

Hit compounds were tested for abilities to inhibit hsDHFR using a test-tube based enzymatic assay (Sigma, CS0340). Briefly, $\sim 1.5 \times 10^{-3}$ units of hsDHFR was combined with assay buffer, NADPH (60 µM, final) and 1 µM hit compound (final) in a 1 mL cuvette. Using this solution, the spectrophotometer (Smart Spec 3000, BioRad, Hercules, CA) was blanked at 340 nm. Next, dihydrofolic acid (50 µM, final) was added and a kinetic read was performed measuring the absorbance at 340 nm every 10 sec for 150 sec. Linear regression was performed on the data using GraphPad Prism and plotted.

Intravitreal Injections

Eight to twelve week old WT Balb/c mice were given an anesthetic cocktail of ketamine/xylazine (120 mg/kg and 16 mg/kg, respectively) followed by application of pupillary dilators, cyclopentolate hydrochloride (1% [w/v]) and tropicamide (1% [w/v]) (Alcon, Fort Worth, TX). After dilation, GenTeal Severe Dry Eye Gel (Alcon) was applied to the cornea to maintain hydration throughout the procedure. Using a stereo microscope (Zeiss, Oberkochen, Germany), the eye to be injected was proptosed and punctured at a 45° angle from the horizontal by a 30G needle at the limbus, followed by the removal of the 30G needle. A 33G, ½" needle fitted to a Hamilton micro-syringe (Hamilton, Reno, NV) containing 2 µL of adeno-associated virus (AAV) encoding for Nano luciferase (NLuc) 2A ecDHFR.firefly luciferase (FLuc) using the AAV2/2 MAX serotype (Reid et al., 2017) (7×10^9 vg), produced and purified by the University of North Carolina Viral Vector Core (Chapel Hill, NC) was used to perform the intravitreal injection. Using an intravitreal injection, this serotype infects layers of the neural retina including the ganglion cell layer, inner retinal neurons, and photoreceptors (Reid et al., 2017). The 33G ½" needle was positioned inside the previous incision at the same 45° angle while the virus was slowly injected over the course of approximately one minute, and then held in place for an additional minute before being removed. Post injection, AK-POLY-BAC antibiotic ointment (Akorn, Lake Forest, IL, USA) was applied topically to the eye, followed by additional GenTeal gel. This procedure was repeated on the contralateral eye using only HBSS with 0.14% Tween (HBSS-T).

Intravenous Tail Vein Injection

Ten to twelve week old WT Balb/c mice were restrained using a Mouse Tail Illuminator Restraint (Baintree Scientific, Baintree, MA) and injected intravenously with a 27G needle through the tail vein with 200 µL of AAV2/8 NanoLuc 2A ecDHFR.Fluc (5×10^9 vg, also produced and purified by the UNC Chapel Hill Viral Vector Core). Intravenous injection of this AAV serotype will primarily transduce hepatocytes.

Oral Gavage

Oral gavage solutions containing stabilizers of interest were prepared by dissolving 1 mg stabilizer in 20 μ l DMSO, followed by 40 μ l PEG-400, 4 μ l Tween-80 (all from Fisher), 20 μ l cremophor (Sigma Aldrich, St. Louis MO), and 116 μ l 5% dextrose in water, in this specific order. Gavage was performed with reusable stainless feeding needles (Braintree Scientific, Massachusetts, USA) in 200 μ l doses.

Bioluminescence Imaging

Baseline ecDHFR DD-firefly luciferase signal was measured the day before small molecule administration by intraperitoneal (i.p.) injection of luciferin (150 mg/kg, Gold Biotechnology, St. Louis, MO) followed by bioluminescent flux measurement over a 20 min time course (IVIS Spectrum, Perkin Elmer, UT Southwestern Small Animal Imaging Resource). One day later, 6 h after small molecule administration by gavage, ecDHFR DD-firefly luciferase signal in the eye or liver was measured. The peak total flux values between the baseline readings and post-gavage values were plotted.

Immunohistochemical Analyses of Microglia in Retinal Flat-Mounts

Mice were euthanized by ketamine/xylazine overdose. Eyes were enucleated and fixed for 2 h in 4% paraformaldehyde at room temperature (RT), then rinsed in PBS. Retinas were then dissected and pre-treated in 0.3% Triton X-100 in PBS for 30 min (x4) and then blocked in 0.3% Triton X-100 in PBS containing 10% goat serum for 2 h at RT. Microglia were labeled using anti-Iba-1 antibody (1:500; #019-19741, Wako, Madison, WI) overnight at 4°C. Following washes in PBS, the retinas were incubated with AlexaFluor488 goat-anti-rabbit (1:1000, #A-11008, Invitrogen, diluted in PBS with Tween) overnight at 4°C and mounted using ProLong Diamond Antifade Mountant (Invitrogen). Twelve Z-stack (2 μ m x 25 steps) images were taken at 25x magnification from peripheral, mid-peripheral and central regions of the four quadrants of each retina using Leica SP8 confocal microscope. The images were Z-projected for maximum intensity using ImageJ (FIJI) and Iba-1 positive cells were counted separately in the inner retina and outer retina using trainable Weka segmentation plugin. Briefly, a Z-projected image was loaded into ImageJ and subjected to Weka segmentation that outlines microglia cell bodies. The image was then run through auto-threshold and converted to a binary image. By applying appropriate particle parameters (i.e., size and circularity) the Analyze particle command was run which gave the output of cell outline and cell count. For each individual retina, the microglia cell count was obtained by averaging the twelve counts for inner and outer retina. Two-way ANOVA statistical analysis was performed to compare cell densities in control and GW2580 treated retinas.

QUANTIFICATION AND STATISTICAL ANALYSIS

Student's t-test statistical analysis was performed using Excel (Office 365, Microsoft, Redmond, WA). Analysis of variance (ANOVA) statistical analyses were performed using Prism (GraphPad, San Diego, CA). Statistical details (n, mean, standard deviation vs. standard error, etc.) of each experiment can be found within the figure legend. Statistical tests were used based on the assumption of a normal distribution.

DATA AND CODE AVAILABILITY

This study did not generate any unique datasets or code.